PHOTOCATALYTIC DEGRADETION OF METHYLENE BLUE AND ANTIBACTERIAL ACTIVITY OF POLYANILINE TIN(IV) MOLYBDOPHOSPHATE COMPOSITE

MSc THESIS

BELAYNEH ASSEFA SIME

APRIL 2018

HARAMAYA UNIVERSITY, HAREMAYA

Photocatalytic Degradetion of Methylene Blue and Antibacterial Activity of Polyaniline Tin(Iv) Molybdophosphate Composite

A Thesis Submitted to the Department of Chemistry,
Postgraduate Program Directorate
HARAMAYA UNIVERSITY

In Partial Fulfilment of the Requirements for the Degree of
MASTER OF SCIENCE IN CHEMISTRY

Belayneh Assefa Sime

Apri 2018
Haramaya University, Haramaya

HARAMAYA UNIVERSITY

POSTGRADUATE PROGRAM DIRECTORATE

I here by certify that I have read and evaluated this Thesis titled **"***Photocatalytic Degradation 0f Methylene Blue And Antibacterial Activity of Polyaniline –tin (IV) molybdophosphate Composite"* by Belayneh Assefa. I recommend that it can be submitted as fulfilling the thesis requirement

Abi Taddesse (PhD)	_____	_____
Major Advisor	Signature	Date
Tesfahun Kebede (PhD)	_____	_____
Co- Advisor	Signature	Date

As members of the Board of Examiners of the MSc Thesis Open Defense Examination, I certify that I have read and evaluated the thesis prepared by Belayneh Assefa and examined the candidate. I recommend that the thesis be accepted as fulfilling the Thesis requirement for the degree of Master of Science in Chemistry (Inorganic Chemistry).

_____	_____	_____
Chairperson	Signature	Date
_____	_____	_____
Internal Examine	Signature	Date
_____	_____	_____
External Examiner	Signature	Date

DEDICATION

To my mother **Bogalech Belete,** my wife **Asnakech Adunga** and my children **Simret, Bezawit, Yilak and Bilen**

STATEMENT OF THE AUTHOR

By my signature below, I declare and affirm that this Thesis is my own work. I have followed all ethical and principles of scholarship in the preparation and compilation of this Thesis manuscript. Any scholarly matter that is included in the Thesis has been recognized through citation. This Thesis is submitted in partial fulfillment of the requirements for an MSc degree at the Haramaya University. The Thesis is deposited in the Haramaya University Library and is made available to borrowers under the rules of the Library. I solemnly declare that this manuscript has not been submitted to any other institution anywhere for the award of any academic degree, diploma, or certificate. Brief quotations from this Thesis may be made without special permission provided that accurate and complete acknowledgement of the source is made. Requests for permission for extended quotations from or reproduction of this manuscript in whole or in part may be granted by the Head of the Department or Director of Postgraduate Program Directorate when in his or her judgment the proposed use of the material is in the interest of scholarship. In all other instances, however, permission must be obtained from the author of the Thesis.

Name: Belayneh Assefa Sime

Signature:_____

Date: _____

Department: Chemistry

BIOGRAPHICAL SKETCH

The author was born on the 29th of June 1970 in Bale Zone, Golelcha wereda at Borat Kebele. He attended his elementary and secondary education in Golelcha and Ginnir Schools respectively. Later, he joined Robe Teachers' Training Institute and graduated with certificate in teaching in 1988. He was then assigned by the Educational Office of Bale zone in Weltei Elementary School. After one year of service, he was transferred to Jara Secondary School where he served as a teacher and laboratory assistant. He joined Adama teachers' collage in distance program in 2001 and received Diploma in chemistry in 2004. He was then transferred to Jara Preparatory School in 2005. He joined Addis Ababa University in the summer program and received B.Ed. degree in chemistry in 2008. He has been teaching in Jara Preparatory School hitherto and joined the Postgraduate Program at Haramaya University to pursue MSc in summer program in Chemistry in July 2011.

ACKNOWLEDGMENTS

I would like to extend my sincere and heartfelt thanks to my major advisor Dr. Abi Taddesse, for his encouragement and genuine guidance from the very beginning of the selection of the research topic till the thesis write up. I have my sincere thanks to my co-advisor Tesfahun Kebede (PhD) for his endless help in correcting, editing, critical assessment and constructive comments and suggestion. Again, I would like to give great respect and heartfelt thanks to Prof. Isabel Diaz and her group for their support in SEM, XRD and Uv-Visible in characterization in the Institute of Catalysis and Petroleum Chemistry (CSIC), Madrid, Spain.

I would like to give great respect and thank to the Department of Chemistry, Haramaya University for giving me access to the laboratory and instrumentation facilities and for characterizing the as-synthesized samples. Special thanks should go to Dr. Ephriem Tadesse for running the PL spectra of the as-synthesized samples. The same goes to the School of Plant Sciences, Haramaya University for their kind cooperation in allowing me to use their laboratory facilities for undertaking antimicrobial studies.

I would like to thank Chemistry Department of AAU for the FT-IR characterization of the as- synthesized samples. The institutional support I got from the Ministry of Education and Oromiya Education Bureau, which they jointly provided me the opportunity to pursue my education and made this study possible, is highly appreciated.

Last but not least, I would like to thank my parents, family members and my friends for their unreserved encouragement and constant support.

ACRONYMS AND ABREVIATIONS

E_g	Band-Gap Energy
CB	Conduction Band
e-CB	Conduction band electron
DMSO	Dimethyl Sulfoxide
FTIR	Fourier transform infrared
PANI	Poly aniline
PANI/TMP	Polyaniline- Tin (IV) Molybdophosphate
RSO	Reactive Oxygen Species
SEM	Scanning Electron Microscope
TMP	Tin(IV)molybdophosphate
VB	Valence band
h+ VB	Valence band hole
XRD	X-Ray Diffraction

TABLE OF CONTENTS

Continues…

Continues…

Continues…

LIST OF TABLES

LIST OF FIGURES

Figure Page

Continues…

LIST OF TABLES IN THE APPENDIX

Appendix Table **Page**

PHOTOCATALYTIC DEGRADETION OF METHYLENE BLUE AND ANTIBACTERIAL ACTIVITY OF POLYANILINE TIN(IV) MOLYBDOPHOSPHATE COMPOSITE

ABSTRACT

Polyaniline-tin (IV) molybdophosphate (PANI /TMP) was prepared using sol–gel method by mixing polyaniline (PANI) gel into the inorganic precipitates of Tin (IV) molybdophosphate (TMP). The composite was characterized by various techniques such as X-ray diffraction, UV-Visible, Fourier transform, scanning electron microscope, photoluminescence. Photocatalytic activities and antimicrobial efficiencies of the bare polymer Polyaniline, the inorganic composite Tin (IV) molybdophosphate and the composite polyaniline- tin (IV) Molybdo Phosphate were evaluated using methylene blue as a model organic pollutant and Gram negative and Gram positive bacteria as test microbes respectively. Photocatalytic and antibacterial activities of Polyaniline - tin (IV) molybdophosphate nanocomposite were found to be the highest. The results obtained indicate the degradation efficiency of 72.96% in 180 min. exposure time using visible light irradiation. Mechanism of scavenger reaction also assure the most important species in the degradation process be ($\cdot O_2$) and ($OH^{\cdot}$). Highest photocatalytic degradation efficiency of the polyaniline Tin(IV) molybdophosphate composite was obtained at initial concentration of 10 ppm MB, 100 mg/L of catalyst load and at pH=8. Antibacterial efficiency of the polyaniline - tin (IV) molybdophosphate support over both Gram negative and Gram positive bacteria were found to be relatively higher than polyaniline and Sn (IV) molybdophosphate.

Keywords: Antimicrobial activity, composite, Methylene blue, Photocatalysts, Polyaniline.

1. INTRODUCTION

Environmental pollution is the major concern of all the human population today. A considerab le percentage of the world's production of dyes is lost during the process of dyeing in the water system. The presence of dyes in the water system is posing a dangerous effect to human beings as well as aquatic life (Aksu, 2005; Asahara *et al*., 2009). Textile industries discharge their dye effluents into the water bodies which affect the physical and chemical nature of natural water and makes it unfit for use. The dyes used in textile industries have complex structure and most of them are mutagenic and carcinogenic to human beings (Kant *et al*., 2014).

Methylene blue ($C_{16}H_{18}$ N_3SCl) is a blue coloured powder which is water soluble and causes different problems in humans such as nausea, hemolysis, hypertension and distress in respiration. Several classical and conventional methods have been used to remove the organic contamination from effluents but are not reliable and effective. The commonly used techniques such as coagulation, microbial degradation, chemical oxidation, adsorption and photocatalysis have been explored for the removal of organic pollutants from the aqueous system (Wang *et al*., 2010). Among these techniques, photocatalysis is the most efficient and consistent method for the degradation of a large variety of organic dyes due to their simplicity, fast degradation and no generation of toxic materials (Anbia and Bharti and Varshney, 2010; Pouretedal *et al*., 2009).

Photocatalysis is the combination of using catalysts and UV/Visible light, for the treatment of waste water and gaseous pollutants. When illuminating a photocatalyst using UV/visible light, various organic compounds can be oxidized and mineralized at the photocatalyst surface in solution at ambient and atmospheric condition. This is because strong oxidation and reduction sites are produced at the photocatalytic surface when it is illuminated with light of the appropriate wavelength, radicals formed at the surface dissolved in solution and then react with pollutants (Chen *et al*., 2007).

Recently, use of nano size polymeric and inorganic ion-exchanger's photocatalytic oxidation to toxic pollutants is being increasingly valued. A lot of organic matter can be decomposed

into inorganic and less toxic simpler compounds. The various types of nanoparticles such as $SrTiO_3$, CdS, Bi_2O_3/Cu_2O, Fe_2O_3 etc. have been investigated as effective photocatalysts for the degradation of organic pollutants (Gupta *et al*., 2013). However, the composite ion exchangers with nano scale dimensions have attracted a great concern due to their varied applications in different fields. A lot of research is done on synthesis of PANI/metal, PANI/ metalloid, PANI/non-metal composites and have been exploited for various electrolytic , photo-catalytic and sensing application (Ciric-Marjanovic, 2013). Conductor and metal-based have been extensively used because of tunable optical properties for photochemical applications (Lu *et al*.,2011). However, conjugated polyenes as PANI may act as sensitizers and also modify physical and chemical properties of metal based materials. PANI has been a popular part of many hybrid nanocomposites.

Nature has provided us with various inorganic and organic ion exchange materials having their own specificity and selectivity. The inorganic ion exchangers are thermally and chemically stable. Organic ion exchangers have good mechanical strength and can be utilized for treatment of large volume of waste effluents. The composite ion exchangers have been given attention in order to encapsulate the desired properties of both organic and inorganic counterparts into one molecule. The nano domain advanced composite ion exchangers have been used in environmental remediation because of their selectivity, specificity and wide range of applicability (Khan and Khan, 2010; Vatutsina *et al.*, 2007).

The unprecedented opportunities in material designing have fuelled rapid development in synthesis of nanostructured composite materials, by using organic polymer and inorganic fillers. Organic–inorganic composites with nano scale dimensions are of growing interest because of their multi functionality, and numerous potential applications such as enhancement of conductivity (Fisher, 2012), toughness (Liu *et al.*, 2012), optical activity ((Jeon and Baek, 2010) catalytic activity (Wang, 1996) and chemical selectivity. The two most promising properties of nano composite ion exchangers being explored in present era of time are antimicrobial activity and photocatalytic activity. In this regard, some of organic-inorganic ion exchanger nano composite used as photocatalytic and antimicrobial activity are polyaniline arsenophosphate, cellulos acetate tin (IV) phosphate, cellulose acetate zirconium (IV) phosphate, polyaniline zirconium(IV) silicophosphate. Recently, we reported a new composite

exchanger polyaniline Sn(IV) molybdophosphate with good selectivity to Cu(II) and Pb(II) ions Bamlaku *et al* (2016). However, there is still a dearth of information on the photocatalytic and antimicrobial application of this composite exchanger. The present work therefore aims to evaluate the photocatalytic and antimicrobial applications of this exchanger. Instruments such as XRD, UV-Vis, FTIR, SEM, and PL were used to characterize the as-synthesized polyaniline supported composite.

General Objective

☞ To evaluate the photocatalytic and antimicrobial activities of polyaniline Tin(IV) molybdophosphate composite.

Specific Objectives

- ❖ To synthesize polyaniline Tin(IV) molybdophosphate composite nanoparticles using sol-gel method.
- ❖ To characterize the as-synthesized photocatalysts using XRD, UV-Vis, SEM-EDX, PL and FTIR techniques.
- ❖ To assess the photocatalytic and antimicrobial activities of the as-synthesized composite.
- ❖ To investigate the effect of operational parameters under photocatalytic degradation studies of methylene blue.

2. LITERATURE REVIEW

2.1 Nano Materials

Nano composites are composites in which at least one of the phases shows dimensions in the nano meter range (1nm = 10^{-9}m).The definition of nano composite material has broadened significantly to encompass a large variety of systems such as one-dimensional, two-dimensional, three-dimensional and amorphous materials, made of distinctly dissimilar components and mixed at the nanometer scale .The general understanding of these properties is yet to be reached. It Changes in particle properties can be observed when the particle size is less than a particular level, called 'the critical size. Additionally, as dimensions reach the nanometer level, interactions at phase interfaces become largely improved, and this is important to enhance materials properties. Nowadays, nano composites offer new technology and business opportunities for all sectors of industry, in addition to being environmentally friendly (Kamigaito *et al*., 1999).

Nano-particles of semiconductors have a great potential as water purification catalysis and redox active media due to their large surfaces, and their size and shape dependent optical, electronic and catalytic properties (Obare and Meyer *et al*., 2004). Environmental pollution had an influence on human survival and development. Nano-particles are of interest because of their high reactivity due to the large surface area to volume ratio. It was observed that nano-materials displayed significantly different properties at nanometer sizes as compared to the properties of the same material in bulk and that the properties of the materials are size and shape-dependent at nano scale range (Caruso, 2001). The large surface area of small-sized particles is expected to be beneficial for photocatalytic reactions that mostly occur on the surface of the catalysts (Kamat *et al*., 1993). Nanocomposites, a high performance material exhibit unusual property combinations and unique design possibilities. Polymeric materials containing metal oxide particles constitute a new class of polymer composites materials. The main purpose of the preparation of the nanocomposite is to obtain the synergic effect of the polymer and the inorganic compound. Nanocomposites have a peculiar structure, i.e. a phase separated structure, with a nanoscale interface between the polymer matrix and the inorganic compound (Nano phase separated structure). This phase separated structure plays a very

important role in the production of a molecular-level synergic effect between the organic and inorganic compounds in nanocomposites. Conducting polymers are combined with metal oxides because of their enhanced physical and electronic properties. Nanocomposite material composed of conducting polymers & oxides have open more field of application such as drug delivery, conductive paints, rechargeable batteries, toners in photocopying, smart windows, etc.

According to their matrix materials, nanocomposites can be classified as ceramic matrix nanocomposites (CMNC), metal matrix nanocomposites (MMNC), and polymer matrix nanocomposites (PMNC). Organic polymer based inorganic nanoparticle composites have attracted increasing attention because of their unique properties emerging from the combination of organic and inorganic hybrid materials. Generally, the resultant nano composites display enhanced optical, mechanical, magnetic and optoelectronic properties. Therefore, these composites have been widely used in the various fields such as military equipment, safety, protective garments, automotive, aerospace, electronics and optical devices (Jeon and Baek, 2010)

2.1.1. Organic Conducting Polymer

Conducting polymers are known for their ability to be compatible with biological molecules in neutral aqueous solutions. Conducting the polymers, such as Polyaniline, polythiophene, polypyrrole, and their derivatives, have been reported as promising sensitizers to extend the spectral response of TiO_2 to visible region (Liang and Li, 2009). Additionally, conducting polymers have the ability to efficiently transfer the electric charges produced by biochemical reactions to electronic circuits. Polyaniline (PANI) is a technologically important conducting polymer due to its unique electrical, electrochemical, and optical properties. (Zhu *et al.*, 2010) reported the hopeful photocatalytic degradation of methyl orange using Polythiophene/Titanium dioxide composites. (Gu *et al.*, 2012) reported the photocatalytic degradation of Rhodamine B using a novel TiO_2/Polyaniline composite. It was found that the prepared composites found to be very efficient photocatalyst under visible light irradiation Moreover, PNAI acted as fast separation channel for photo generated carriers to significantly improve the separation efficiency of the electron-hole.

2.1.2. Polyaniline (PANI)

The continuously growing interest in the study of PANI over the years is mainly because of its diverse, but unique properties of PANI, allowing its potential applications in various fields. among all the conducting polymers, polyaniline is known for it' ease of synthesis, environmental stability and, easy to dope by photonic acids. The term Polyaniline corresponds to a class of polymers having up to 1000 repeat units (also called mers). There are several reports of polyaniline found in the literature over the decades about the structure and constitutional aspect of aniline polymerization. Polyaniline can be synthesized by both chemical and electrochemical oxidative polymerization.

The conducting polymers have emerged as a new class of materials because of their unique electrical, optical and chemical properties. By proper doping the conductivity of these materials can be varied from semiconducting to metallic regime. Polyaniline has been studied extensively due to its ease of synthesis in aqueous media. Due to its environmental stability, and special electrical and optical properties. Polyaniline can be prepared in three major forms that differ in the degree of oxidation (Y) (the ratio of amine nitrogen over the total number of nitrogen atoms). For the fully reduced Leucoemeraldine base (LEB) that Y is one, the half oxidized emeraldin base (EB),Y is 0.5 and for fully oxidized Pernigraniline base (PNB),Y is 0 as in Figure 2. Polyaniline is an insulator in each of these forms with a band gap around 3.6 eV. These polymers can also exist in the corresponding. protonated (salt) forms but only emeraldin salt (ES) has shown high electrical conductivity .The structure of the Polyaniline (PANI) chain can be expressed by the general formula (Salma *et al*.,2009)

$$[(-B-NH-B-N-)_y\ (-B-N=Q=N-)_(1-Y)\ ]_X$$

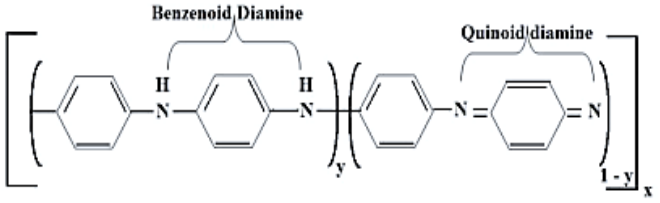

Figure 1.Structure of polyaniline

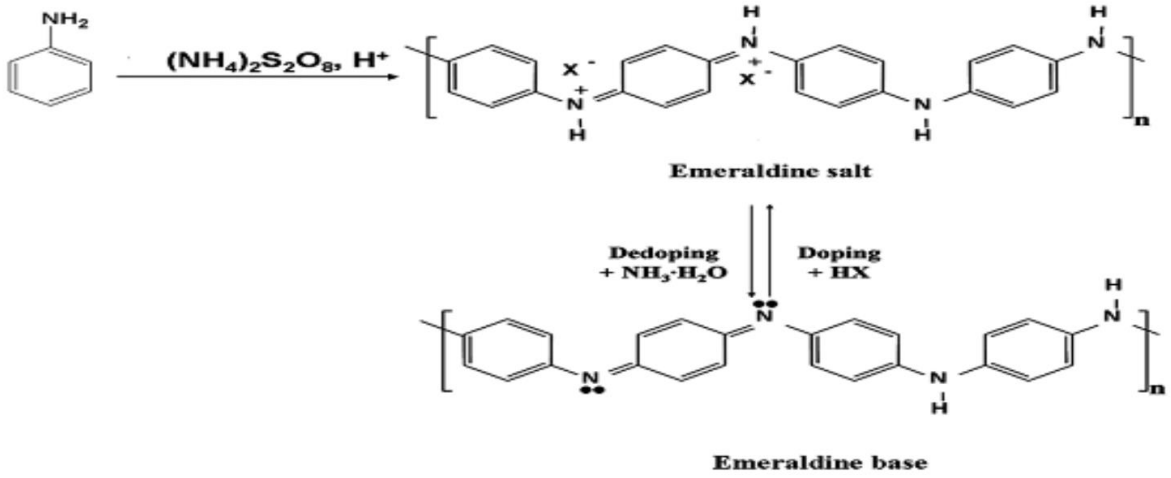

Figure 2. Reaction scheme for PANI chemical synthesis

2.1.3. Organic-inorganic (O-I) Nanocomposites

Nano-ordered composite materials consisting of organic polymers and inorganic materials have been attracting attention for the purpose of the creation of high performance or high-functional polymeric materials. Especially, the word of "polymer hybrid" claims the blends of organic and inorganic components at nano-level dispersion. Significant effort is focused on the ability to obtain control of the nanoscale structures via innovative synthetic approaches. The properties of nanocomposite materials depend not only on the properties of their individual parents, but also on their morphology and interfacial characteristics. Structure-property correlations in polymer nanocomposites have been extensively dealt which describes the mechanical properties of polymers based on nanostructure and morphology. It is possible to synthesize a uniform polymer hybrid using "in-situ polymerization method" of polymerizing organic monomers as well as forming an inorganic matrix by a sol -gel reaction. The merit of this method is that, compared to the organic polymer, the monomer has superior solubility and dispersibility, and hence it is easy to obtain a more uniform hybrid. The sol-gel reaction makes possible to incorporate the organic polymer segments in the network matrix of inorganic materials. The interaction between the organic polymer and the inorganic matrix in a polymer hybrid can be done by using:

i. Hydrogen Bonding

ii. π-π interaction

iii. Ionic interaction

The PANI based composite has been synthesized by different method to improve its properties (Wang *et al.*, 2001; Sanchez *et al*., 2001; Wu *et al*., 2007). In PANI based composite a good balance can be achieved between electrical and mechanical properties. Therefore the interest has arisen for preparation of polyaniline and pectin based composite material having utility for the removal of metal ions, dyes and bacteria from the water system. The inorganic ion exchangers are thermally and chemically stable. Organic ion exchangers have good mechanical strength and can be utilized for treatment of large volume of waste effluents. The composite ion exchangers have been given attention in order to encapsulate the desired properties of both organic and inorganic counter parts into one molecule. The nano domain advanced composite ion exchangers have been used in environmental remediation because of their selectivity, specificity and wide range of applicability (Khan and Khan, 2010; Vatutsina *et al.*, 2007).

2.1.4. Polyaniline- Tin (IV) Molybdophosphate Composite

Polyaniline-tin (IV) molybdophosphate has bifunctional nature and strong acidic cation Exchanger. The material is thermally stable in terms of ion exchange capacity since it retains about 75% of its ion exchange capacity up to 600 °C (Bamlaku *et al.*, 2016)

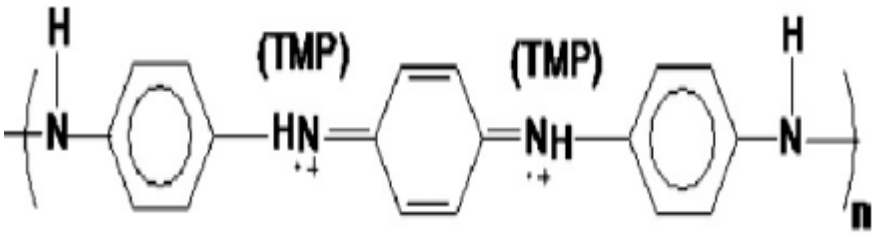

Figure 3. Structure of Polyaniline- Tin (IV) molybdophosphate composite

2.2. Photocatalysis

From the beginning of the 21st century there has been an increasing demand for the implementation of clean energy technologies rendering little or no environmental footprint. However, until such time that clean, non-carbon based energy becomes a reliable and

affordable commodity, environmental pollution abatement for a multitude of everyday industrial and domestic activities remains a crucial responsibility. Amongst the many abatement strategies known, semiconductor mediated photocatalysis has been a subject of vigorous academic research for the past 20 years. Due to the largely insoluble nature of the catalysts during application, the area of semiconductor photocatalysis invariably constitutes a heterogeneous catalytic system that adheres to the five discrete processes associated with conventional heterogeneous catalysis:

1) Transfer of liquid or gaseous phase reactants to the catalytic surface
2) Adsorption of at least one reactant
3) Reaction in the adsorbed phase
4) Desorption of product(s).
5) Removal of products from the interface region

Photocatalysis is a rapidly developing field of research with a high potential for a wide range of industrial applications, which includes mineralization of organic pollutants, disinfection of water an air, production of renewable fuels and organic synthesis. A great deal of attention has been devoted in the last years to photocatalytic processes both in the homogeneous phase and in heterogeneous systems. In its broadest sense, photocatalysis concerns the use of light to induce chemical transformations on organic or inorganic substrates that are transparent in the wavelength range employed. Radiation is absorbed by a photocatalyst whose electronically excited states induce electron- or energy-transfer reactions able to trigger the chemical reactions of interest (Hennig *et al.*, 1993; Kisch, 1989). Photocatalysis process, as an environmental application is a relatively novel subject with tremendous potential in the near future. It can be defined as the acceleration of photoreaction in the presence of a catalyst. The initial interest in the heterogeneous photocatalysis was started when Fujishima and Honda discovered in 1972 the photochemical splitting of water into hydrogen and oxygen with TiO_2 (Fujishima and Honda, 1972). From this date extensive work has been carried out to produce hydrogen from water by this novel oxidation reduction reaction using a variety of semiconductors. In heterogeneous photocatalysis two or more phases are used in the photocatalytic reaction. A light source with semiconductor material is used to initiate the photoreaction. The catalysts can carry out substrate oxidations and reductions simultaneously. UV light of long wavelengths can be used, possibly even sunlight (Fox and Dulay, 1993).The

concept photocatalysis and, of greater importance here, heterogeneous photocatalysis were first introduced in the second decade (1910–1920) of the 20th century.

Heterogeneous photocatalysis is an advanced oxidation process which is the subject of a huge amount of studies related to environment recovery, such as air cleaning and water purification, in which organic and inorganic pollutants are totally degraded to innocuous substances over mainly TiO_2 photocatalysts. It also includes a large variety of reactions: mild or total oxidations, dehydrogenation, hydrogen transfer, oxygen-18 and deuterium isotopic exchange, metal deposition, water detoxification, gaseous pollutant removal, bactericidal action etc. In line with the last point, it can be considered as one of the new ‘‘Advanced Oxidation Technologies’’ (AOT) for air and water purification treatments. (Bhatkhande *et al.*, 2001)

Attributes of an ideal photocatalyst for heterogeneous photocatalysis are

1. Stability and sustained photo activity
2. Biologically and chemically inert, nontoxic
3. Low cost
4. Suitability towards visible or near UV light
5. High conversion efficiency and high quantum yield
6. Can react with wide range of substrate and high adaptability to various environments
7. Good adsorption in solar spectrum (Fujishima *et al*., 2000)

During the last two decades much attention has been paid to the reactions that take place on the illuminated surface of semiconductor metal oxides and sulfides. These compounds, mainly TiO_2, ZnO, CdS, WO_3, etc., are semiconductors, i.e. they have a moderate band-gap between their valence and conduction bands. Under illumination by photons of energy greater than band gap energies, the valence band electrons can be excited to the conduction band, creating highly reactive electron-hole pairs. After migration to the solid surface, these may undergo electron-transfer processes with adsorbates of suitable redox potentials. In this way, these semiconductor compounds act (if the reaction exhibits a positive free energy gain), or catalytic photoassisted reactions (negative gain).

Infectious diseases are the leading cause of death worldwide, accounting for nearly one half of all deaths in tropical countries which are also becoming a significant problem in all countries. Microbial infections are great challenge to human health concern and it is even exacerbated by the growing resistance to the conventional drugs (Ibezim, 2005). Thus, many researchers are

resorting to date to find remedy from nanomaterials for infectious diseases. Development of new antimicrobial agents is among the proposed solution to this problem.

2.3. Principles of Photocatalytic Degradation

In the photocatalytic degradation process, organic pollutants are destroyed in the presence of Semiconductor photocatalyst an energetic light source and oxidizing agent such as oxygen or air. Only photons with energies equal or greater than the band gap energy can result in excitation of valence band (VB) electrons which then promote the possible reactions with organic pollutants. The absorptions of photon with energies lower than the band gap energy usually cause dissipation in the form of heat. The illumination of the photo catalyst with sufficient energy leads to the formation of positive hole (h^+) in the valence band and an electron (e^-) in the conduction band (CB). The positive hole oxidizes either the pollutants directly or water to produce hydroxyl radical $HO^{\cdot}$ whereas the electron in the conduction band reduce the oxygen adsorbed on the photo catalyst (Ahmed *et al*., 2010).

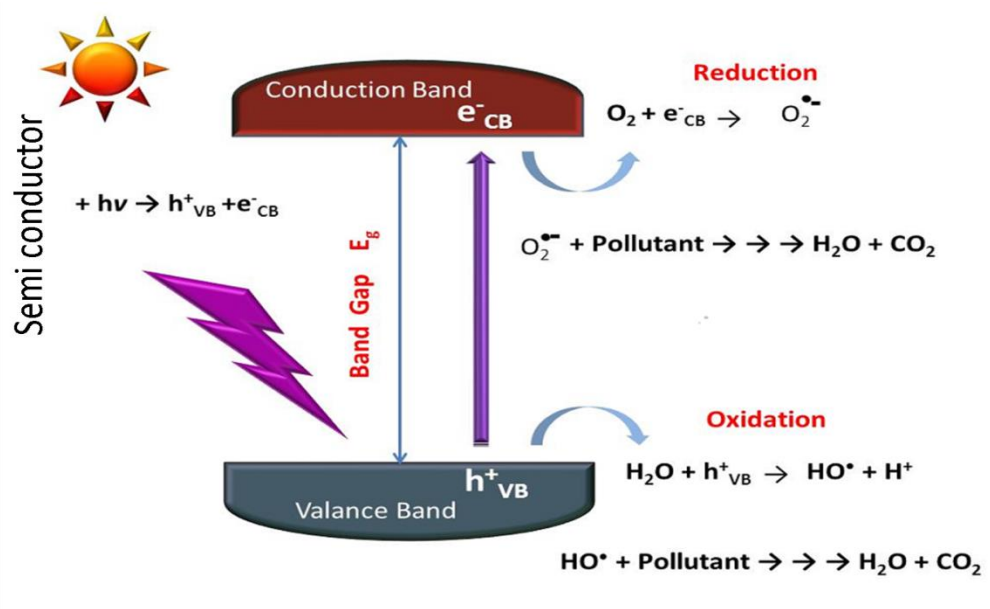

Figure 4. Mechanism of semiconductor photocatalysis

Hydroxyl radical generation by the photo catalytic oxidation process is shown in the above steps. In the degradation of organic pollutants, the hydroxyl radical generated from the oxidation of adsorbed water is the primary oxidant, and the oxygen present react with electron

at the conduction band to form peroxide radicals followed by a number of steps forming H_2O or OH radical thus prevent the recombination of an electron-hole pair. The hydroxyl radical attacks compounds resulting in various reaction intermediates depending on the nature of the compound. The resulting intermediates further react with hydroxyl radical to produce final degradation products as carbon dioxide and water. In the photo catalytic degradation of pollutants, when the reduction process of oxygen and the oxidation of pollutants do not advance simultaneously, there is an electron accumulation in the CB thereby causing an increase in the rate of recombination of $e^-$and h^+(Hoffman *et al*., 1995; Herrmann, 1999).The basic reaction of above mentioned process are as follows:

In the degradation of organic pollutants, the hydroxyl radical which is generated from the oxidation of adsorbed water is the primary oxidant and the presence of oxygen at CB prevents the electron –hole pair recombination (Ahmed *et al*., 2010).

$$h\nu \xrightarrow{\text{semiconductor}} e^- + h^+$$

$$H_2O \longrightarrow H^+ + OH^-$$

$$h^+ + OH^- \longrightarrow OH\cdot$$

$$h^+ + H_2O \longrightarrow OH\cdot + H^+$$

$$e^- + O_2 \longrightarrow O_2^-$$

$$O_2^- + H^+ \longrightarrow OH_2\cdot$$

$$2OH_2\cdot \longrightarrow O_2^- + H^+$$

$$H_2O_2 + O_2\cdot \longrightarrow OH\cdot + H_2O_2$$

$$H_2O_2 + h\nu \longrightarrow 2OH\cdot$$

$$\text{Organic polutent} + OH\cdot + O_2 \longrightarrow CO_2 + H_2O + \text{Heat}$$

Adsorbed oxygen at grain surface is an electron capture, which can restrain the combination of electron and hole. The nano scale catalysts have higher photocatalytic activity than normal material (Zhang *et al*., 2001). There are two reasons for this:

2.3.1. Quantum Size Effect

When the particle diameter becomes less than a certain critical value, the valence band and conduction band change into discrete levels, the energy gap become broader, means, the valence band electric potential becomes more positive and the conduction electric potential becomes more negative. Then the oxidation reduction capability of the electron and hole is enhanced and the photocatalytic activity of nano semiconductor is improved (Zhang *et al*., 2001).

2.3.2. Specific Surface Area

At higher specific area of particles there are more atoms on the surface, it improve the adsorption capability of semiconductor for organic pollutants: the time spent by electrons and holes to get to the surface of the particle is decreases. The smaller the particle diameter, the shorter is time spent by carriers diffusing from inside to the surface. It can get higher separated efficiency and lower probability of electron holes recombination. Therefore, the nano semiconductor has more photocatalytic efficiency than the common semiconductor (Zhang *et al*., 2001).

2.4. Properties and Application of Photocatalyst

There is almost no limit to the combinations of inorganic and organic components in the formation of hybrid materials. Therefore materials with novel composition-property relationships can be generated that have not yet been possible. Based on the increased importance of optical data transmission and storage, optical properties of materials play a major role in many high-tech applications. The materials used can reveal passive optical properties, which do not change by environmental excitation, or active optical properties such as photochromic (change of color during light exposure) or electrochromic (change of color if electrical current is applied) materials. Silica is preferred as the inorganic component in such

applications because of its low optical loss. Other inorganic components, for example zirconia, can incorporate high refractive index properties, or Titania in its rutile phase can be applied for UV absorbers. Functional organic molecules can add third order nonlinear optical (NLO) properties and conjugated polymers, conductive polymers can add interesting electrical properties. The enhancement of mechanical and thermal properties of polymers by the inclusion of inorganic moieties, especially in the form of nanocomposites, offers the possibility for these materials to substitute classical compounds based on metals or on traditional composites in the transportation industry or as fire retardant materials for construction industry (Kickelbick, 2007). Organic–inorganic hybrid materials do not represent only a creative alternative to design new materials and compounds for academic research, but their improved or unusual features allow the development of innovative industrial applications . Nowadays, most of the hybrid materials that have already entered the market are synthesized and processed by using conventional soft chemistry based routes developed in the eighties. Lo oking to the future, there is no doubt that these new generations of hybrid materials, born from the very fruitful activities in this research field, will open a land of promising applications in many areas: optics, electronics, ionics, mechanics, energy, environment, biology, medicine for example as membranes and separation devices, functional smart coatings, fuel and solar cells, catalysts, sensors, etc.

The two most promising properties of nanocomposite ion exchangers being explored in present era of time are antimicrobial activity and photocatalytic activity. The photocatalysis is one of the efficient methods to eradicate organic waste problem. Thus researchers are focusing on newer photocatalytic agents with higher efficiency. The nanocomposite ion exchangers are new class of multifunctional-advanced materials which have been successfully employed as photocatalyst (Gupta *et al.*, 2013). It has been shown to be useful for the destruction of micro-organisms such as bacteria and viruses for the inactivation of cancer cells, for odor control, for the photo splitting of water to produce hydrogen gas, for the fixation of nitrogen and for the cleanup of oil spills.

To treat organic pollutants containing wastewater we require multifunctional-advanced materials such as nano composite ion exchangers. The various organic polymers are used as organic part including guar gum, polyaniline, pectin, cellulose, polystyrene and polyacrylamid

e etc. in ion exchangers which act as adsorbent for dyes. These polymeric parts increase the surface area and provide mechanical strength to inorganic counterpart. On the other hand, the inorganic counterpart is responsible for photocatalytic activity of the material. These nano composite ion exchangers had multifunctional applications in environmental remediation such as adsorption, photo catalysis, chromatography and ion selective electrode etc. (Gupta *et al.*, 2014).

Recently, polyaniline zirconium (IV) silicophosphate (PANI–ZSP) nanocomposite ion exchanger was prepared using sol–gel method (Pathania *et al*., 2014). The nanocomposite ion exchanger was utilized as photocatalyst for the remediation of methylene blue dye from water. It was also successfully used as an antibacterial agent against *Escherichia coli*.

Guar gum - cerium (IV) tungstate nanocomposite (GG/CTNC) cationic exchanger was used as potential adsorbent for the remediation of methylene blue. The correlation coefficient value indicated a good fit of monolayer Langmuir model to the adsorption of methylene blue. The adsorption kinetic study revealed that the adsorption process followed the pseudo second order kinetics (Gupta *et al*., 2014).

Pectin-thorium (IV) tungstomolybdate (Pc/TWM) nanocomposite was synthesized and characterized using different techniques. The nanocomposite was explored for antibacterial and photocatalytic activities. 76% of methylene blue dye was photo catalytically degraded after five hours exposure (Gupta *et al*., 2013)

2.5. Photo excited Electron–Hole Separation Process in Organic-inorganic Composite

In a typical mechanism on absorption of a photon, an electron is promoted from the valence band, into the conduction band, leaving a hole behind. Excited state conduction-band electrons and valence-band holes can recombine and dissipate the input energy as heat, get trapped in metastable surface states, or react with electron donors and electron acceptor adsorbed on the semiconductor surface. In the absence of suitable electron and hole scavengers, the stored energy is dissipated within a few nanoseconds by recombination. If a suitable scavenger or surface defect state is available to trap the electron or hole, recombination is prevented and

subsequent redox reactions may occur. The valence band holes are powerful oxidants while the conduction-band electrons are good reductants. Most organic photodegradation reactions utilize the oxidizing power of the holes either directly or indirectly (Wang *et al*., 2010; Pouretedal *et al*., 2009).

PANI/ZSP polyaniline - Zr(IV) silicophosphate) nanocomposite ion exchanger acts as absorbent for dyes from water. The dye gets adsorbed on the nanocomposite ion exchanger, then the nanocomposite ion exchangers irradiated with visible light. The particle gets excited to generate hydroxyl and superoxide radicals (as the material contains Zr and poly aniline which generates free radicals (Fan *et al*., 2008). The free radicals so generated disrupt the conjugation in the adsorbed dye molecules and hence degrades the dye. The proposed mechanism for the photo catalytic degradation of dye was shown as follows:

PANI -ZSP + MB Dye ↔ PANI –ZSP- Dye

PANI - ZSP -Dye + hv → PANI –ZSP (e^- +h^+) Dye

PANI –ZSP (h^+) + H2O →PANI –ZSP ($OH^\bullet$) + H^+

PANI –ZSP (h+) +OH^- → PANI –ZSP ($OH^\bullet$)

PANI –ZSP (e^-) + O_2 → PANI – ZSP ($O^\bullet_2$)

$OH^\bullet$+ Dye→ Intermediate Product → Degraded Product

$O^\bullet_2$+ Dye → Intermediate Product →Degraded Product

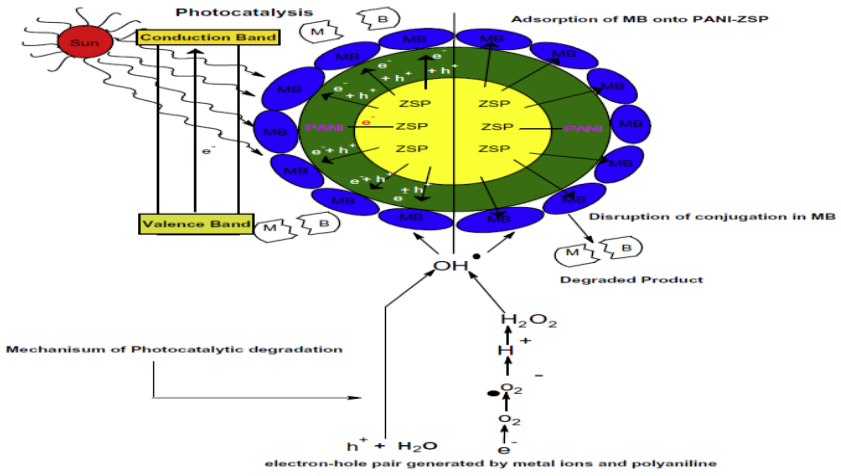

Figure 5. Photocatalytic degradation of methylene blue dye onto PANI/ZSP nanocomposite ion exchanger (Fan.Y. *et al.*, 2008)

2.6. Factors Affecting Photocatalytic Process

There are different factors which may affect photocatalytic efficiency of photocatalysts under UV as well as solar radiation. Some of these are: Substrate (Dye) initial concentration, photo catalyst amount, temperature, band gap of photo catalyst, and pH.

2.6.1. pH of the Solution

pH of the solution also affects the rate of photo degradation of the dye by changing the surface charges of the nano photocatalyst particles. Hence adsorption of charged particle at the surface of catalyst is altered which changes the rate of degradation reaction. Photocatalyst surface may protonate or deprotonate with the change of pH value. Anionic dyes will be degraded more at lower pH. Reductive cleavage may take place in azo dyes at low pH favoring the degradation of azo dyes (Soutsas *et al*., 2010).

Organic compounds in wastewater differ greatly in several parameters, particularly in their speciation behavior, solubility in water and hydrophobicity. While some compounds are uncharged at common pH conditions typical of natural water or wastewater, other compounds exhibit a wide variation in speciation (or charge) and physic-chemical properties. At pH below its pKa value, an organic compound exists as a neutral species. Above this pKa value, organic compound attains a negative charge. Some compounds can exist in positive, neutral, as well as negative forms in aqueous solution. This variation can also significantly influence their photocatalytic degradation behavior. pH of the wastewater can be varied significantly. pH of aquatic environment plays an important role on the photocatalytic degradation of organic contaminants since it determines the surface charge of the photocatalyst and the size of aggregates it forms (Bahnemann and Haque, 2007). The surface charge of photocatalyst and ionization or speciation (pKa) of an organic pollutant can be profoundly affected by the solution pH. Electrostatic interaction between semiconductor surface, solvent molecules, substrate and charged radicals formed during photocatalytic oxidation is strongly dependent on the pH of the solution. In addition protonation and DE protonation of the organic pollutants can take place depending on the solution pH. Sometimes protonated products are more stable under UV Irradiation than its main structures (Saien and Khezrianjoo, 2008).Therefore the pH

of the solution can play a key role in the adsorption and photocatalytic oxidation of pollutants. The ionization state of the surface of the photocatalyst can also be protonated and deprotonated under acidic and alkaline conditions respectively.

2.6.2. Photocatalyst Load

Heterogeneous photocatalysis is influenced by the concentration of photocatalyst. ·OH radicals are increased with the increase in concentration of photocatalyst resulting decolonization of the dye. After a certain limit of time concentration of catalyst solution become opaque and light radiation cannot enter in to activate the catalyst particles. Hence the rate of dye degradation decreased (Sun *et al.,* 2008).

2.6.3. Initial Dye Concentration

Photocatalytic degradation of those molecules of dye take place which are adsorbed on the surface of photocatalyst particles, whole of the dye molecule do not degrade. If the dye concentration is increased the number of dye molecule in the solution is increased which affect the degradation rate. Hence for the optimum degradation rate, the concentration of dye should not be increased after certain limit (Wang *et al*., 2008).

2.7. Degradation of Organic Pollutants by Photocatalysts

The photo generated electron-hole pairs diffuse to the nanoparticle surface before recombination to initiate a chain of photochemical reactions (Yang *et al*., 2013). Photocatalytic process resulted in the oxidation–reduction and finally the degradation of a wide variety of organic pollutants through their interaction with photo generated holes or reactive oxygen species, such as $\bullet OH^-$ and $\bullet O_2^-$ radicals. The advanced oxidation process initiated by photocatalytic degradation has offered a better solution for decolourization, breakdown and mineralization of dyes. Styrene based ion exchangers have been recorded cost effective, easily process able, renewable and excellent material for remedial applications (Khan *et al*., 2002; Varshney and Tayal, 2001). Polymer based nano composites have been used as excellent photocatalyst as the polymer surface of the catalyst helps to transfer the

photo generated electrons and holes and prevents the electron hole pair recombination (Ahmed *et al*., 2010)

2.8. Property of Methylene Blue Dye

Methylene blue (C16H18 N3SCl) is a dark green crystalline solid and dissociates in aqueous solution into methylene blue cation and the chloride ion. The removal of methylene blue from wastewater is of great significance due to the serious environmental harm (Altaher and ElQada, 2011)

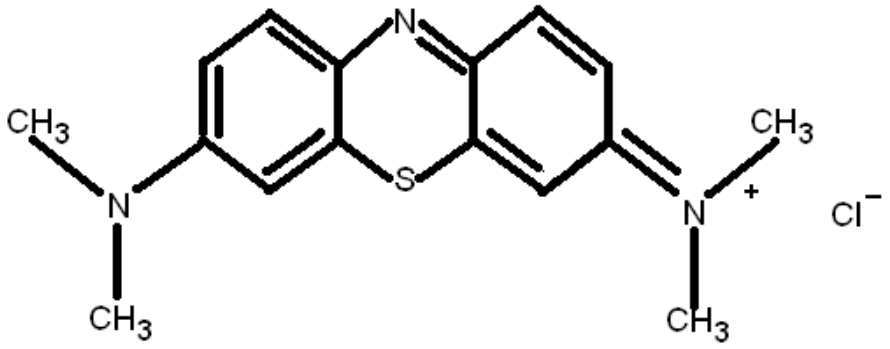

Figure 6. Chemical structure of methylene blue

Methylene blue (methylthionine chloride) is a heterocyclic aromatic chemical compound with the chemical name bis (dimethylamino)-phenazathionium chloridetetramethylthionine chloride (Wiklund, 2007. methylene blue (MB) is a cationic thiazine dye that is deep blue in the oxidized state while it is colorless in its reduced form (leucomethylene blue). MB and leucomethylene blue exist as a redox couple in equilibrium and together form a reversible oxidation- reduction system or electron donor-acceptor couple (Miclescu and Wiklund, 2010)

2.9. Methods of synthesizing Nanomaterials

There are a number of methods to synthesis the nano sized photocatalysts used for the photocatalytic activities as well as antimicrobial application. Some of these are given below.

2.9.1. Precipitation Method

Precipitation is the creation of a solid. When the reaction occurs in a liquid solution, the solid formed is called the precipitate. The chemical that causes the solid to form precipitation is called the precipitant. Without sufficient force of gravity (settling) to bring the solid particles together, the precipitate remains in suspension. Sometimes the formation of a precipitate indicates the occurrence of a chemical reaction. For example silver nitrate solution is poured into a solution of sodium chloride, a chemical reaction occurs forming a white precipitate of silver chloride. When potassium iodide solution reacts with lead nitrate solution, a yellow precipitate of lead iodide is formed. Precipitation may occur if the concentration of a compound exceeds its solubility (such as when mixing the solvents or changing their temperature). In solids, precipitation occurs if the concentration of one solid is above the solubility limit in the host solid, due to rapid quenching or ion implantation, and the temperature is high enough that diffusion can lead to segregation into precipitates. Precipitation in solids is routinely used to synthesize (Dhar, 2007). Precipitation reactions can be used for making pigments, removing salts from water in water treatment, and in classical qualitative inorganic analysis. Precipitation is also useful to isolate the products of a reaction during work up. Ideally, the product of the reaction is insoluble in the reaction solvent. Thus, it precipitates as it is formed, preferably forming pure crystals.

2.9.2. Sol-gel Method

The precipitation methods always have the disadvantage that the stoichiometry of the precipitate(s) may not be exact if one or more ions are left in solution. The sol-gel method overcomes this because the reactants never precipitate out. First, a concentrated solution or colloidal suspension of the reactants, the ‘sol’, is prepared, which is then concentrated or matured to form the ‘gel’. Those colloids, which contain small particles (1–1000 nm in diameter), could be highly chemically homogeneous. A sol is a colloidal suspension of particles in a liquid; for the materials being discussed here, these particles will typically be 1 to 100 nm in diameter. A gel is a semi-rigid solid in which the solvent is contained in a framework of material which is either colloidal (essentially a concentrated sol) or polymeric. To prepare solids using the sol-gel method, a sol of reactants is first prepared in a suitable liquid. Sol preparation can be either simply the dispersal of an insoluble solid or addition of a

precursor which reacts with the solvent to form a colloidal product. A typical example of the first is the dispersal of oxides or hydroxides in water with the pH adjusted so that the solid particles remain in suspension rather than precipitate out. A typical example of the second method is the addition of metal alkoxides to water; the alkoxides are hydrolyzed giving the oxide as a colloidal product. The sol is either then treated or simply left to form a gel over time by dehydrating and/or polymerizing. To obtain the final product, the gel is heated. This heating serves several purposes it removes the solvent, it decomposes anions such as alkoxides or carbonates to give oxides, it allows rearrangement of the structure of the solid, and it allows crystallization to occur. Both the time and the temperature needed for reaction in sol-gel processes can reduced from those in the direct ceramic method; in favorable cases, the time from days to hours, and the temperature by several hundred degrees. (Lesley and Elaine, 2005).

Among the various methods, sol-gel method has attracted more attention because of low process cost, easy control of composition, suitable for scale-up and relatively low calcinations temperatures. The main disadvantages of the sol-gel process include a broad size distribution and a high concentration of defects. Therefore, this synthesis technique is used sparingly. (Debasis *et al*.2010).

2.9.3. Hydrothermal Method

Some of the developed techniques for the synthesis of metal oxide particles use high temperature (above 500 ^{0}C) or pressures greater than atmospheric or combination of both variables. These synthesis methods often lead to the formation of micron-sized-objects and can produce special shapes such as rods, ribbons, flowers ,etc. (Kar *et al*.,2006).

2.9.4. Impregnation Method

Catalyst support is the material, usually a solid with a high surface area, to which a catalyst is affixed. The activity of heterogeneous catalysts and nanomaterial-based catalysts occurs at the surface atoms. Consequently, great effort is made to maximize the surface area of a catalyst by distributing it over the support. The support may be inert or participate in the catalytic reactions. Typical supports include various kinds of carbon, alumina, silica and organic

polymer (Zhen and Francisco, 2006). In impregnation techniques, the support is contacted with a precursor solution, in other word impregnation is related to ion exchange (adsorption processes) and the interaction with the support is dominant. Thus, low loadings, often for precious metals, are achieved by adsorption of the precursor molecules onto surface groups of the support (ion adsorption) or through the exchange of ions in, for example, zeolites (ion exchange), after which excess precursor is removed. When higher loadings are required, the washing step is skipped and the support is directly dried, so that all precursor ends up on the support (impregnation and drying). Impregnation can be performed to incipient wetness, whereby the pores of the support are filled with precursor solution, to prevent deposition on the external surface of the catalyst grains and to limit waste (Munnik *et al.*, 2015)

2.10. Characterization of Nanocomposite

2.10.1. X-ray Diffraction Method

In order to determine the crystal phase composition and the crystallite size of the photocatalyst a powder X-ray diffraction method (XRD) study should carried out. X-ray diffraction is a nondestructive analytical technique that can be applied for the identification of unknown specimens and for the determination of materials properties. It is the most important and beneficial technique in solid state chemistry and it has been applied for the finger print characterization of crystals and for the determination of their structures. This method requires an X-ray source (monochromatic or of variable), the sample (single crystal, powder or solid piece) which is under investigation and a detector (radiation counter or photographic film) that takes the diffracted X-rays (Ece, 2012).

2.10.2. UV-Visible Absorption Method

The optical absorption plays an important role in the photocatalysis, especially in the visible-light photodegradation of contaminants. Based on the diffuse absorbance spectra of the materials, the absorption edge wavelength and band gap energies of the as-synthesized samples were determined and compared. The wavelength at the absorption edge for a semiconductor is determined as the intercept on the wavelength axis for a tangential line drawn on the absorption spectrum (Escobedo *et al*., 2007).

Diffuse reflectance spectroscopy is a sensitive technique which uses the interaction of light, absorption and scattering to produce characteristic spectrum providing information regarding the structure and composition of the material. Electronic transition in materials can be observed in liquid state using Uv-Visible spectroscopy. But in the case of insoluble solids, Uv-Visible diffuse reflectance is used. It is used to study the electronic transitions between orbitals or bands in the case of atoms, ions and molecules in gas, liquid or solid state. This technique is performed on the basis of electronic excitation by the absorption of light (Klaas *et al*., 1997).

2.10.3. Fourier-Transformed Infrared Spectroscopy (FTIR) Method

FTIR spectroscopy is conducted to identify the functional groups present on nanoparticles (Gupta *et al*., 2013). Using FTIR analysis, the infrared emission spectrum, absorption, photoco nductivity, or Raman scattering of a solid, liquid, or gas can be evaluated. The spectrum represents a fingerprint of the nanoparticles consisting of absorption peaks that correspond to the frequencies of vibrations between the bonds of atoms in the nanoparticle. Since each type of nanoparticle contains a unique combination of atoms, we can identify functional groups present inside the nanoparticles based on the FTIR spectra. The number of functional groups present in the nanomaterial can be determined by the size of the peaks of the spectrum. The transmission spectra for the nanoparticles are obtained by the formation of thin, transparent potassium bromide (KBr) pellets containing the compound of interest.

The KBr mixtures are placed in a vacuum line overnight prior to pellet formation, and the pellets are again placed in the vacuum line before use. The transmission spectra are obtained after purging in dry air and background corrected relative to a reference blank sample (KBr). Commonly, the vibrational spectroscopy covers a wave-number ranging from 4000-400 cm^{-1} which is used to excite stretching and bending molecular vibrations (Silverstein and Webster, 2002).

2.10.4. Scanning Electron Microscopy

SEM is a type of electron microscope which provides the information about sample's surface topography, composition and other surface properties such as electrical conductivity. In

scanning electron microscopy (SEM), it is possible to observe and characterize the heterogeneous organic and inorganic materials on a nanometer (nm) to micrometer (μ m) scale. A three-dimensional-like image of the surfaces of a very wide range of materials can be taken. The basic constituents of the SEM are the lens system, electron gun, and electron collector, visual and photo -recording cathode ray tubes (CRTs) and associated electronics. In scanning electron microscope technique, the electrons from a focused beam are restored across the surface of the material. Then, electrons reflected by the surface of the sample and emitted secondary electrons are detected in order to give the surface topography of like catalysts, polymers and crystals. It is a common method for examining the particle size, magnetic domains, crystal morphology, and surface defects. SEM is a widely accepted technique to extract structural and chemical information point-by-point from a region of interest in the sample. It is generally employed to examine the surface morphologies of the material at higher magnifications. It is an inevitable tool in heterogeneous catalysis because most of the reactions are taking place on the surface (Bootz *et al*., 2004). Secondary electrons, backscattered electrons, diffracted backscattered electrons, photons; visible light and heat are the major constituents of the signals produced from the SEM instrument. Among these, secondary electrons are responsible to produce the surface image of the sample (Gupta *et al*., 2013).

2.10.5. Photoluminescence (PL)

Spectroscopic and electro analytical techniques are used to evaluate the efficiency of charge separation and characterization of the hetero structure. Photoluminescence (PL) spectra helped us to trace the fates of the photo generated electron/hole pairs. For effective photocatalytic reaction the photo generated electron/hole pair should follow the first path, thus, should not recombine. PL spectroscopy concerns monitoring the light emitted from atoms or molecules after they have absorbed photons (Skoog and Leary, 1992). It is suitable for materials that exhi bit photoluminescence. PL spectroscopy is suitable for the characterization of both organic and inorganic materials of virtually any size, and the samples can be in solid, liquid, or gaseous forms. The sample's PL emission properties are characterized by four parameters: intensity, e mission wavelength, bandwidth of the emission peak, and the emission.PL is mainly used as a diagnostic and development tool in semiconductor research, since it can provide information

about the electronic structure and the emission mechanism of the material (Tao *et al*., 2017).The emission intensity of the as-synthesized nano composites was characterized by PL.

3. MATERIALS AND METHODS

3.1. Experimental Site

Synthesis of polyaniline, Tin(IV) molybdophosphate and the composite polyaniline-Tin(IV) molybdophosphate; the degradation experiment, photoluminescence characterization of the nonmaterial, were conducted at Haramaya University Chemistry Department Research Laboratory. The antimicrobial properties of the as-synthesized nanomaterials were conducted in the School of Plant Sciences at Haramaya University. FTIR analysis was done at Addis Ababa University, Department of Chemistry and UV-Vis, XRD and SEM-EDX were conducted at the Institute of Catalysis and Petroleum Chemistry (CSIC), Madrid, Spain.

3.2 Apparatus and Instruments

Some of apparatuses and instruments used in this study include: X-ray diffraction patterns of as-synthesized semiconductors were obtained using X pert pro pananalytical Diffractrometer, CSIC Madrid, Spain using X-ray diffractrometer equipped with a Cu target Kα radiation (wavelength 1.5406 Å). The measurements were made at room temperature and the accelerating voltage and the applied current were 40 kV, 30 mA, respectively. The instrument was operated under step scan type with step time and degree (2θ) of 1s and 0.020°, respectively, for the range of 10° to 80°. Absorption spectra measurements of the as-synthesized powders were made using UV-Vis spectrophotometer (Sanyo, SP65, Galanakamp, UK), by scanning over 200-800 nm. The morphology of the solids and particle distribution were determined by scanning electron microscopy (SEM) using a Hitachi TM1000 with EDX detector. The FTIR spectrum of the samples was determined using the KBr disk method. The IR absorption pattern was recorded between 400 and 4000 cm^{-1} using SHIMADZU (1730, Japan) spectrometer. The prepared samples were characterized based on their spectra photoluminescence obtained using fluorescence spectrometer (Scimadzu, RF5301 Florimeter). Other apparatus like Analytical balance (OHAUS, made in Switzerland), Oven (Contherm 260M), pH meter (MP 220), Deionizer (B114), Orbital shaker S01 (Stuart, UK), beakers, mortar and pestle, ceramic crucibles, volumetric flasks, Pipettes and magnetic stirrer test tubesglss rods filter papers funnels, were also used. For the desired purposes.

3.3. Reagents and Chemicals

Since all chemicals used in were of analytical grade (Sigma-Aldrich) and they were used without further purification. These includes aniline ($C_6H_5NH_2$) , ammonium peroxodisulfate $(NH_4)_2S_2O_8$) Hydrochloric acid (HCl) (36 - 37 % BDH chemicals Ltd, England), tin(IV) Chloride ($SnCl_4$.$5H_2O$), phosphoric acid (H_3PO_4), sodium molybdate (Na_2MoO_4. $2H_2O$), nitric acid (HNO_3 (69 % LR, Breck land Scientific Supplies, U.K), ammonia solution , demineralized water, methyl blue ($C_{16}H_{18}$ N_3SCl) (Mueller-Hinton agar Merck, Germany), Sodium hydroxide (NaOH) (97.5 % BDH chemicals Ltd, England), Sodium Nitrate ($NaNO_3$), methanol (CH_3OH) (97% fine chemical) Phenolphetaline (BDH, England), DMSO (Abron Chemicals India).

3.4. Methods and Procedures

3.4.1. Synthesis of Polyaniline

Polyaniline was synthesized by chemical polymerization method (Bamlaku *et al.*, 2016). The polyaniline was prepared by mixing 10% (v/v) aniline and 0.1 M ammonium peroxo-di-sulfate $(NH_4)_2S_2O_8$ (in 1 M HCl) at 1:1 volume ratio with constant stirring. The pH of the resultant mixture was kept between 0 and 1. The mixture was maintained below $10\ ^0C$ for 1 h.

3.4.2. Synthesis of Tin (IV) molybdophosphate

Tin(IV) molybdophosphate was prepared by mixing equal volumes (50 Ml) of the solutions of $SnCl_4$ $5H_2O$.(0.2M), H_3PO_4 (0.1 M) and Na2MoO_4.$2H_2O$ (0.1 M).The pH of the resulting gel was adjusted by adding 1M HNO_3 or 1M ammonia solution to maintain pH (1) with constant stirring for 1h (Bamlaku *et al.*,2016) .

3.4.3 .Synthesis of polyaniline-Tin (IV) Molybdophosphate nanocomposite

Polyaniline-tin (IV) molybdophosphate nanocomposite was prepared by sol –gel method. The gel of polyaniline was added into the inorganic precipitate of tin (IV) molybdophosphate and mixed thoroughly with constant stirring for 1h (Bushra *et al.*, 2015). The gelatinous precipitate formed was allowed to stand for 24 h in the mother liquor for digestion. The supernatant liquid

was removed and the remaining solid was washed with demineralized water and dried in an air oven at 50 °C (Bamlaku *et al.,* 2016). The dried as-synthesized polyaniline Tin (IV) molybdophosphate was then crushed and packed for photocatalytic and antimicrobial studies.

3.5. Characterization of Photocatalysts

3.5.1. Determination of Point of Zero Charge (pH pzc)

The pH pzc of the as-synthesized nanocomposite was determined by adding 100 mg of the powder into 250 mL beaker. 50 mL of 0.001M $NaNO_3$ was added and adjusted to different pH ranging from 2-12 using dilute HNO_3 or NaOH solutions. The solution was equilibrated for 60 minutes in a mechanical shaker to determine the initial pH. Then, 1g of $NaNO_3$ was added to the above solution and further equilibrated for another 60 minute after agitation to measure the final pH. A plot of ΔpH = pH final- PH initial (Y-axis) versus pH final (X-axis) was used to determine the point of zero charge where the graph intersects the X-axis (Panumati *et al*., 2008).

3 5.2. X-ray diffraction (XRD) study

In order to determine the crystal phase composition and the crystallite size of the photocatalyst, a powder XRD study was carried out. X-ray diffraction patterns of as-synthesized semiconductors were obtained X pert pro pan analytical Diffractrometer, CSIC Madrid, Spain using a using X-ray diffractrometer equipped with a Cu target Kα radiation (wavelength 1.5406 Å). The measurements were made at room temperature and the accelerating voltage and the applied current were 40 kV, 30 mA, respectively. The instrument was operated under step scan type with step time and degree (2θ) of 1s and 0.020°, respectively, for the range of 10° to 80. The XRD measurement was provided theta (2θ) and the radiation wavelength (λ) and the average crystalline sizes of as-synthesized nanoparticles was calculated by using Debye Scherrer formula.

$$D = \frac{0.94\lambda}{\beta \cos\theta} \qquad \textbf{(7)}$$

Where D is crystallite size in nm, K is the shape factor constant which is equal to 0.94, λ is the x-ray wave length, and FWHM is the full width at half maximum (in radians) for a diffraction occurring at 2θ (in degrees) θ is the Bragg diffraction angle.

3.5.3. Determination of Optical Band Gap

UV–Vis diffuse absorption spectroscopy was carried out to investigate the optical properties of the different photocatalysts. For the determination of absorption edge and band gap energy of the as-synthesized photocatalysts, UV diffuse absorption was measured using SP65 spectrophotometer at scanning over λ = 200-800 nm. Band gap energy of the as-synthesized photocatalysts was obtained using the relation (El-Kemary *et al.*, 2010) given bellow.

$$E_g = \frac{1240}{\lambda} \qquad (8)$$

Where, E_g is band gap energy and λ is maximum wavelength (nm) corresponding to absorption edge of nanoparticles.

3.5.4. Fourier transform infrared (FTIR) Study

The infrared spectrum of the as-synthesized powder PANI, TMP and PANI /TMP nanocomposite was determined by using a FTIR spectrometer at room temperature (Li *et al.*, 2007) from the vibrational infrared spectra extending in the range of 4000 to 400 cm^{-1}. Appropriate amount of nanocomposite was grinded and mixed with KBr. Then percent transmittance of nanocomposite was read in the above range and recorded.

3.5.5. Scanning Electron Microscope (SEM)

The morphologies and particle size distribution of the synthesized PANI, TMP and PANI /TMP products were characterized by the scanning electron microscope images registered using HITACHI Tabletop Microscope TM-1000 with EDX detector to do the elemental analysis.

3.6. Photocatalytic Degradation of Methylene Blue

The photocatalytic activities of the as-synthesized materials for the degradation of methylene blue dye were investigated under visible radiation. All photocatalytic degradation experiments were carried out in duplicate at room temperature. For this purpose, required amounts of the as-synthesized photocatalyst powder and 100 mL of aqueous solution of MB were taken in a reactor tube. The mixture was stirred first in dark for 30 min to obtain adsorption/desorption equilibrium before illumination. During the illumination of the sample by visible radiation, air was purged into the solution with the help of porous tube. Then 10 ml of sample was withdrawn at 20 min interval of time and centrifuged at 3000 rpm for 5 min and filtered to remove the catalyst particles before measuring absorbance. The absorbance of the clear solution was measured at maximum absorption wavelength (λ_{max} = 665nm) using Uv-Vis spectrophotometer for quantitative analysis. Photocatalytic degradation of methylene blue dye using the nano composite photocatalysts was monitored spectrophotometrically (Hong *et al*., 2009) Percent degradation (% degradation) of methylene blue dye was finally calculated using the following formula:

$$\% \text{ Degradation } = \frac{C_O - C}{C_O} \times 100 \qquad (9)$$

Where, C_o is dye initial concentration, C is the concentration of dye at irradiation time.

3.7. Factors Affecting Photocatalytic Degradation of Dye

3.7.1. Effect of pH

Photocatalytic degradation of methylene blue dye was studied using photocatalysts load 100 mg/L and initial concentration of 10 ppm over pH of 2-12 using λ_{max} 665 nm. The pH of the reaction mixture was adjusted by using nitric acid and ammonia solutions.

3.7.2. Effect of Photocatalyst Load under Visible Light

The optimum amount of photocatalyst required for maximum degradation of methylene blue dye was examined by varying the amount of photocatalyst from 10 to 400 mg/L for the given

concentration of dye (10 ppm) and pH (8). The blank experiment was done without photocatalyst to examine the extent to which methylene blue dye was photolyzed in the presence of light source and without light source to examine the extent to which methylene blue dye was photolyzed in the presence of catalyst.

3.7.3. Effect of Initial Concentration of Methylene Blue

To observe the effect of dye initial concentration (C_o), photocatalytic degradation of methylene blue was studied using dye concentration 10 to 30 mg/L of 100 ml solution at optimum catalyst load (100 mg/L) and optimum pH (8) of reaction mixture.

3.8. Antimicrobial Studies

The synthesized polyaniline tin (IV) molybdophosphate (PANI/TMP) nanocomposite was tested *in vitro* for its antibacterial activity by using the paper disc diffusion method. Antibacterial studies was conducted against four important bacteria, *Escherichia coli and Salmonella typhus* (Gram-negative) *Staphylococcus aureus* and *S. coccus (*Gram-positive), using nutrient agar medium. A *Chloramphenicol* standard antibiotic drug was used as reference in anti-bactericidal studies. The effectiveness of the compounds was determined by measuring the diameter of inhibition zones (Yadav *et al*., 2011).

3.8.1. Preparation of Media

Bacteria, *Escherichia coli, Salmonella typhus , Staphylococcus aurous* and *S .caucus* was transferred from the culture and then streaked on Mueller Hinton agar (MHA) plate and incubated for 24 h at 37 ℃ in an oven. Then the bacteria were transferred to autoclaved MHA that was maintained at 45 ℃ in a water bath and mixed by vigorous swirling of the flasks. The medium was then poured to sterilized petri dishes, solidified and used for biotest.

3.8.2. Preparation of Sample Solutions

Solutions was prepared by dissolving their 0.1g samples in 10 mL DMSO and their 10/20 μL aliquots was used for biotest

3.8.3. Procedure for Antibacterial Activity Test

Whatmann No.1 filter paper was punctured with office puncture to get 6 mm diameter paper discs. The discs were sterilized in an oven at 180 ^{0}C for 1 h. Then 10µL and 20 µL of solution of compounds were released over paper discs in three replications. The paper discs impregnated with the samples was transferred with sterile forceps to nutrient agar plate seeded with bacteria and incubated at 37^{o}C for 24 h.

4. RESULTS AND DISCUSSION

4.1. Physical Characterization Nanocomposite

4.1.1. Study of Point of Zero Charge

The PZC is a point at which the surface charge of the photocatalyst is zero or neutral that lies in the pH range of 4.5 - 7.0, depending on the catalysts used. Due to the absence of any electrostatic force between photocatalyst and dye particles, the interaction (adsorption) and photocatalysts processes are very less at PZC. When the pH of the system is less than the PZC, the surface charge of the photocatalyst is positive and interaction with the anionic dye is higher and the adsorption and photocatalysis are higher. But when the pH of the system under study is higher than the PZC, the photocatalyst surface will be negatively charged and the repulsion between the photocatalyst and anionic dye particles is higher and adsorption and photocatalysis will be less. If the dye is cationic (MB) at pH greater than the PZC, interaction and photocatalysis is higher but at pH less than the PZC of the photocatalyst the repulsion is higher and the photocatalysis is lesser (Mohamed, 2011).

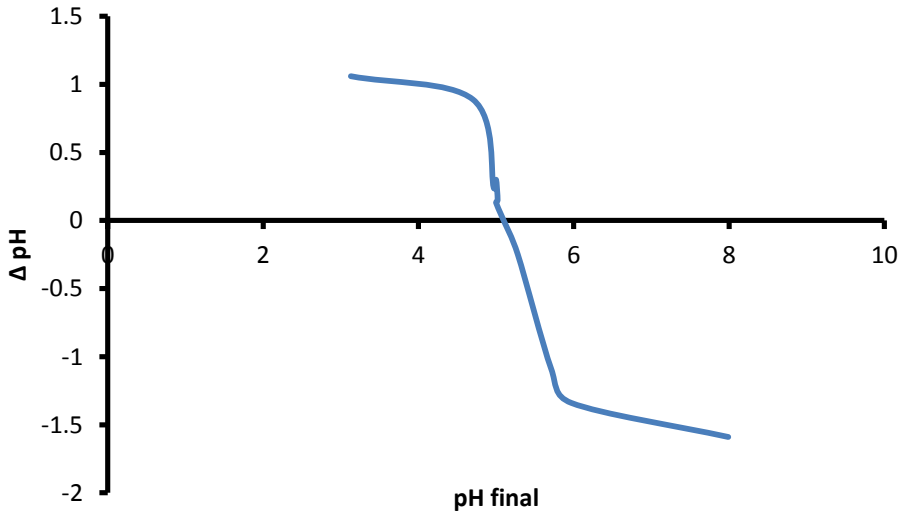

Figure 7. Plot of Point of Zero Charge of PANI /TMP

As illustrated in (Fig. 7), the point of zero charge of polyaniline Tin (IV) molybdophosphate was investigated between pH of 2.0 and 12.0. The PZC of the photocatalyst was found to be 5.09, which is expected to be the point at which the surface charge of polyaniline tin(IV) molybdophosphate is neutral. The photodegradation result revealed that higher adsorption and hence higher photocatalysis was obtained at pH above the PZC of the catalyst, which is pH = 8.0. This is due to the higher interaction between the negatively charged surface of the photocatalyst particles and the positively charged (cationic) MB molecules at this pH. At a pH = 8.0, complete bleaching (decolorizing) of the photocatalyst was observed.

4.2. Physico chemical Characterization of the as-Synthesized Nanocomposite

4.2.1. XRD Pattern Analysis

The X-ray diffraction patterns of the as-synthesized samples polyaniline (fig. 7a) show Peak at 2θ values 9.44°, 15.27°, 20.17°, 25.48°, 27.26°, 35.07°, 44.76° , 27.26°, 35.07°, 44.7° could be attributed to pure PANI. The two broad peaks centered at 2θ= 20.17° and 25.4° are ascribed to the periodicity parallel and perpendicular to the polymer chain and indicated that the pure PANI was in semi-crystalline phase (Sandhya and Sugunan, 2014). Generally polymers are considered to be amorphous, but here the synthesized polymer is showing crystalline structure due to its benzenoid and quinoid functional groups (Srinivas *et al*., 2012). The XRD patterns of the as-synthesized samples of Tin (IV) molybdophsphate (Fig. 8b) shows weak intensity peaks at 2θ values 10.79°, 15.17°, 21.52°, 26.49°*, 30.7°, 32.57°,.36.22°, 36.32°, 39.45°, 44.03°, 44.66° 48.10°, 52.06°, 55.71°, 62.79°, 64.98° representing monoclinic structure. In the XRD pattern of PANI Tin (IV) molybdophosphate composite, the peaks at 2θ = 9.4°, 15.27°, 16.9° and 27.26° of the PANI disappeared while the peak at 20.17° became weaker. The result suggests the addition of nano crystalline hampers during the crystallization of the polyaniline molecular chain. This is because when the deposited polyaniline is adsorbed onto the surface of Tin (IV) molybdophosphate the nano particle, due to the restrictive effect of the surface of nanoparticles and the interaction of PANI and Tin (IV) molybdophosphate nanoparticles, the molecular chain of adsorbed polyaniline is tethered, and the degree of crystallinity decreases.

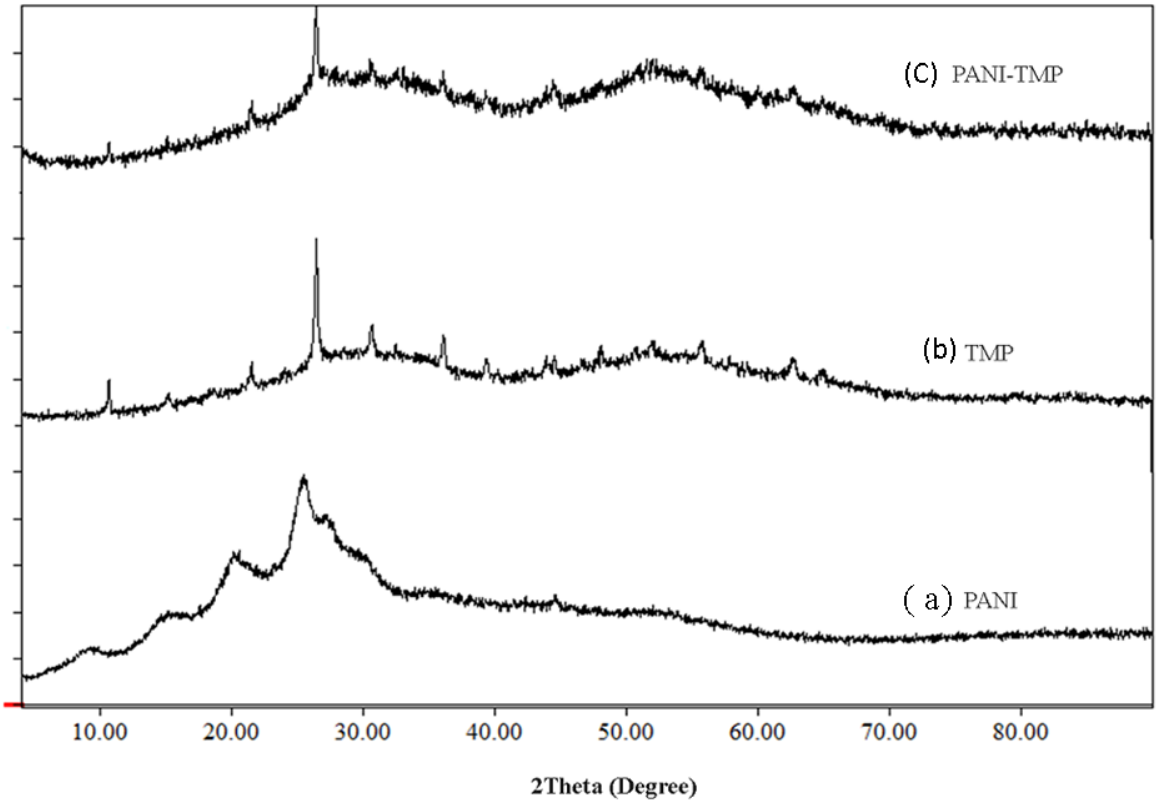

Figure 8. XRD patterns of (a) PANI (b) TMP (c) PANI /TMP

The average crystallite size is calculated by Debye Scherer equation. (Lv *et al*., 2011)

$$D = \frac{0.9\lambda}{\beta \mathrm{Cos}\theta} \qquad (11)$$

Where: β = is full width of half maxima (FWHM),

D = volume weighted crystallite size,

K = Scherrer constant (0.96), λ = wavelength of the X-ray

θ = Bragg angle for the peak at 2θ

The average particle size of samples are tabulated in Table.1

Table 1. Average particle size of PANI, TMP and PANI /TMP samples

Sample	2θ (Degree)	β (Radian)	Particle size (nm)
PANI	25.36	0.0028	49.53
TMP	26.49	0.0027	52.75
PANI-TMP	26.43	0.0031	45.24

4.2.2. UV-Visible Spectra of the as-Synthesized Nanocomposite

UV–Vis diffuse reflectance spectra of PANI, TMP and PANI/TMP were obtained from plot of absorbance against wavelength (Fig. 8 b). The intercept of the tangent line on the descending part of the absorption peak at the wavelength axis gives the value of diffuse absorption edge (nm). Estimation of band gap using the above approach sometimes may not provide clear tangential line when the peak is not well resolved for the samples. This could probably happen when the scattering effect is as high as the optical absorption processes. In such case scattering screens the absorption peak, making the assignment of band gap energy (E_g) uncertain. To avoid the difficulties in obtaining band gap energy (E_g) from UV–Vis absorption spectroscopy in dispersed samples, the diffuse reflectance spectroscopy (DRS) was used and the data obtained as such was transformed using the equation given below (Cao *et al*., 2012) so as to suppress the band gap estimation obtained from plot of absorbance against wavelength.

$$\alpha h\nu = A\,(h\nu - E_g)^{n/2} \qquad (12)$$

Where α, hν, A, and Eg are optical absorption coefficient, the photonic energy, proportionality constant, and band gap energy respectively. This equation the value of n is dependent on the type of transition in a semiconductor as (n=1, direct absorption; and n=4, indirect absorption). By applying n = 1, the direct band gaps of the prepared photocatalysts were determined from the plot of (αhν) ½ versus hν as indicated in the inset of (fig. 8a). Accordingly, the estimated band gaps by extrapolating the straight line to the x-axis for PANI, TMP, and PANI /TMP are obtained as 2.7, 3.1 and 2.1 eV, respectively. This is in good agreement with the result obtained by Salma *et al.* (2009), it can be seen that, when both PANI and TMP are compared with PANI TMP, the later exhibits more red-shift by absorbing in the visible region. The band gap energy (E_g) of Sn(IV) molybdophosphate which is about 3.1 eV, the weak degradatio

n of inorganic molecules in pure Sn(IV) molybdophosphate is due to the poor light absorption under visible irradiation. PANI has a narrower band gap, showing strong absorption in the range from visible to near infrared light (Sandhya, 2014). PANI TMP composite not only can strongly absorb the UV light but also can absorb the visible and near IR light. It is obvious that the composite has higher response over the whole range of Uv–Vis spectrum. The electrons in π-orbital of PANI are excited to π*-orbital by visible light and can readily inject into the CB of Sn(IV) molybdophsphate because the energy level matched well for the charge transfer.Thus,as the charge separation is enhanced by this phenomenon electrons in Sn(IV) m olybdophosphate (CB) would react easily with water and oxygen to produce reactive oxygen species (ROS), which are capable initiating efficiently the chain reaction for the degradation.

As shown in (Fig. 9b) the sharp absorption onseting at 210 nm corresponds to the fundamental absorption edge of the Sn(IV) molybdophosphate nanoparticles. In the absorption spectra of polyaniline (Fig. 8 b), three distinctive peaks of polyaniline appear at about 337, 369 and 607.5 nm, which are attributed to the π–π*, polaron- π* and π- polaron transition (Mehto *et al.*, 2017) respectively. From (Fig. 9 b), it can be noted that the characteristic peaks of nano Sn (IV) molybdophosphate and polyaniline all appear in polyaniline Sn(IV) molybdop hosphate composite. A broad peak in the range 550 - 884 nm, indicates the presence of the PANI on the surface of PANI- Sn(IV) molybdophosphate nanoparticles. The observed red shift in the absorption bands of composite may be due to the interaction of Sn(IV) molybdoph osphate nanoparticles with polyaniline.The result indicates that polyaniline is capable of sensi tizing Sn(IV) molybdophsphate efficiently and the resulting nanocomposite photocatalyst can be activated by absorbing both the ultraviolet and visible light (λ= 225 – 880 nm) to give a maximum chance for visible light harvesting, and this makes it a promising photoelectric conver photocatalytic material for the efficient use of light, especially visible light.

Table 2 Absorbance, maximum wavelength, band gap of synthesized photocatalyst

Sample	Absorbance	Maximum wavelength (nm)	Band gap (E_g) (eV)
PANI	31.1	338.5	2.7
TMP	22.2	210.0	3.1
PANI/TMP	14.0	225.3	2.1

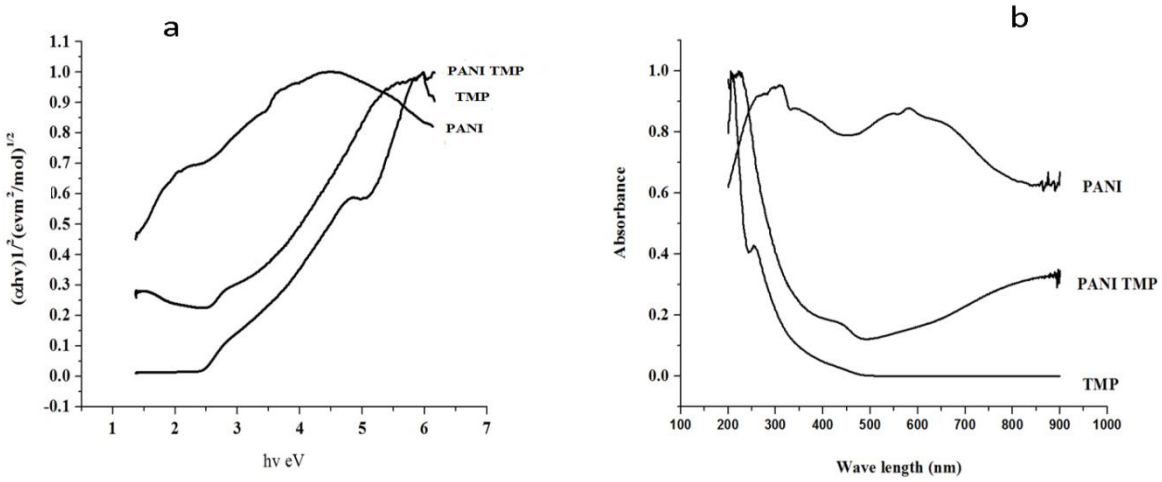

Figure 9. UV- Vis diffuse absorption spectra of PANI, PANI/TMP and TMP using (a) the modified Kubelka-Munk (KM) function and (b) absorbance versus wavelength

4.2.3. Analysis of the FTIR spectra

The infrared spectrum of the Sn(IV) molybdophosphate is recorded in (Fig. 10a). The peak at ≈ 3437 cm^{-1} is characteristics of the stretching mode of water and OH groups adsorbed on Sn(IV) molybdophosphate (Ahmed. *et al*.,2011). The peak at ≈ 1630 cm^{-1} represents the bending mode of water molecules (Acharya *et al*., 2010). The peak at ≈ 1412 cm^{-1} is due to the deformation vibration of hydroxyl groups (M-OH deformation vibration) (Nabi *et al*., 2007). The band at 1370 cm^{-1} can be attributed to the C=O residue probably due to atmospheric CO_2 (Chira *et al*., 2011). The peak at ≈ 1063 cm^{-1} is due to phosphate group (may be due to the presence of PO_4^{3-}, HPO_4^{2-}, H_2PO_4 (Yavari ., 2014). The two peaks at

≈ 600 and ≈ 520 cm^{-1} are associated with metal oxygen bonds are assigned to Sn-O-Sn and Sn-O (belonging to Sn-OH groups) stretching vibration respectively(Yavari.,2014).

The FTIR spectra of as-synthesized sample PANI are shown in (Fig. 10b). The peaks at 3437 cm^{1-} exhibits a broad band, which is attributed to asymmetric and symmetric–OH stretching which are contributed by water molecules adsorbed by the nanomaterial (Ahmed. *et al*., 2011). The peak observed in the 1630 cm^{-1} is attributed to the presence of H-O-H bending vibration of adsorbed water molecule (Acharya *et al*., 2010). The bands at 1598 and 1474 cm^{-1}can be quinoid and benzenoid ring deformation respectively. The bands at 1304 and 1148 $cm^{-1}$are due to the C-N stretching vibration and N-Q-N (Q represents the quinoid ring), respectively. The peak at 2923 cm^{-1} occurs because of aromatic N-H bending. The peak around 2855 cm^{-1} is assigned to residual organic component asymmetric and symmetric C-H stretching mode frequencies. The vibration peak at 1112 cm^{-1} is attributed to C-N double bond stretching. The band characteristic of conducting protonated form is observed at 1245 cm^{-1}.The peak observed around 1384cm^{-1} arise from the absorption of atmospheric carbon dioxide .The peak observed around 744cm^{-1} attributed to C-H out of bending (Kavitha *et al*., 2012).

FTIR spectrum of PANI/TMP (Fig. 10c) exhibits a broad band in the region of 3400cm^{-1}, which is attributed to asymmetric and symmetric–OH stretching. The peak at 2926 cm^{-1} occurs because of aromatic N-H bending. The peak at 1620 cm^{-1} is attributed to the H–O–H bending of water molecules (Acharya *et al*., 2010).The band at 1556 cm^{-1} may be due to the presence of benzinic–quinonic N and the band at 1479 cm^{-1} may be due to aromatic C = C vibration. The band at 1400 cm^{-1} is attributed to the presence of δ (POH). These bands indicate the presence of structural hydroxyl groups exchanging sites (H^+ of the ^-OH groups). The band at 1303 cm^{-1} can be ascribed to stretching vibration of aromatic C–N bond. This may indicate that polyaniline tin (IV) molybdophosphate contains a considerable amount of aniline. Abroad peak at 1053 cm^{-1} may be due to the presence of PO_4^{3-}, $HPO_4^{2-}$and $H_2PO_4^-$ which is attributed to the presence of p-O stretching. A peak~890cm^{-1} is due to the presence of molydate group. The presence of bands at ~511 and ~575 cm^{-1} regions may relate to Sn–O bond vibrations (Bamlaku *et al.,* 2016). The change in intensities of characteristics peaks in PANI/TMP nanocomposite compared to TMP ion exchanger clearly indicated the incorporation of polyaniline into the inorganic counterpart (Fig. 10 c).

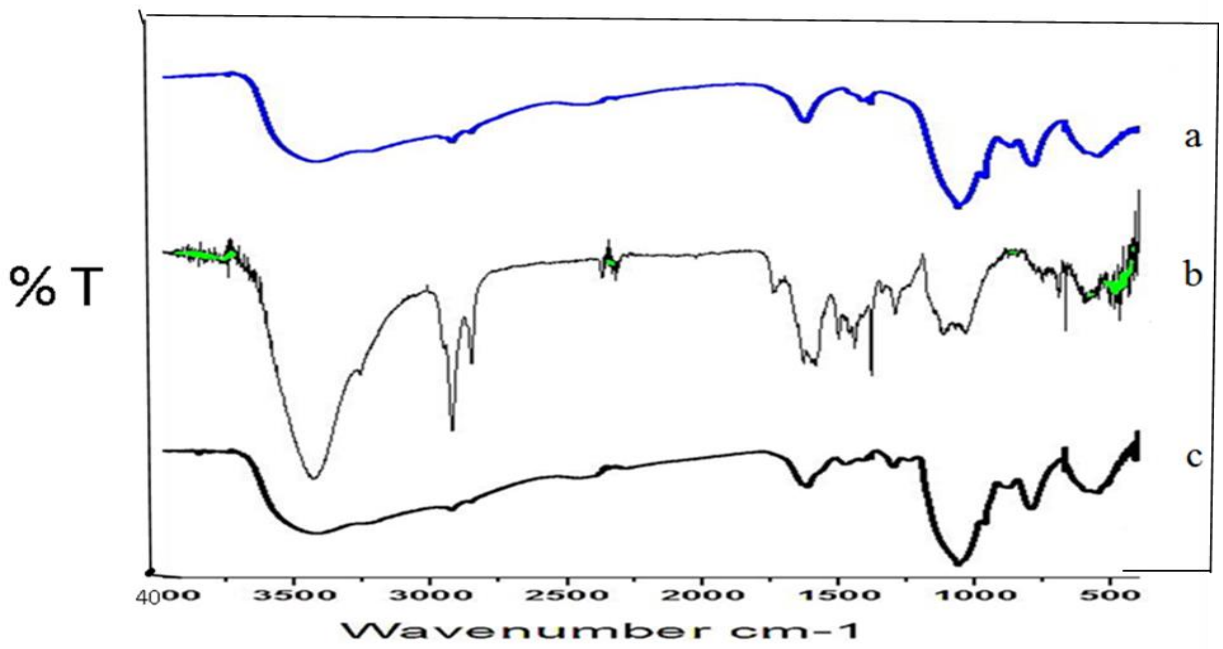

Figure 10. Infrared spectra of the prepared spectra of the prepared (a) TMP (b) PANI and (c) PANI /TMP

4.2.4. Photoluminescence (PL) Study of as-Synthesized Photocatalysts

Photoluminescence (PL) emission spectra were used to investigate the efficiency of charge carrier trapping, immigration and transfer and the fate of electron-hole pairs in semiconductor particles.Polyaniline, Tin (IV) molybdophosphate and Polyaniline- tin (IV) molybdophosphate With excitation wavelength of 310 nm are shown in (Fig. 11). It is well known that the recombination of electron hole pairs can release energy in the form of PL emission. Therefore, lower PL intensity indicates slower recombination of charge carriers, leading to higher photocatalytic activity (Katsumata *et al*., 2014). So, in this study it was clearly observed that the lower PL emission spectrum was recorded for polyaniline tin (IV) molybdophosphate.

The bare Tin(IV) molybdophosphate showed the highest PL emission intensity, indicating that electrons and holes were more easily recombined. However, the PL emission intensity decreased greatly in the case of conducting polymer hybridized Tin (IV) molybdophosphate photocatalysts. So it indicated that the conducting polymer-nano Tin (IV) molybdophosphate

nano composites have lower recombination of electrons and holes. Furthermore, it can be deduced that the photo-produced electrons of the excited conducting Polymer.

Tin (IV) molybdophosphate molecules may transfer more easily and effectively to the conduc tion band (CB) of the Tin (IV) molybdophosphate which reasonably leads to a higher photocatalytic activity since the photo degradation reactions are evoked by these charge carriers. Photoluminescence effect is present as the result of direct radiative recombination, lower recombination of generated carriers causes the decrease of light emission intensity. The order of intensityis, Tin (IV) Molybdophosphate > polyaniline >polyaniline Tin(IV) molybdop hosphate. It is in good agreement with the results obtained for photocatalytic degradation Curves presented in (Fig. 11). Similar results have been reported by Sandhya and Sugunan (20 14) for TiO_2–PANI composite. Polyaniline- tin (IV) molybdo phosphate nanocomposite using the excitation wavelength of 310 nm is given in (Fig. 11). It is observed that the band edge luminescence peak of the composite was slightly red shifted. The observed red shift may also be due to the ionic interaction of PANI with Tin(IV) molybdophosphate.

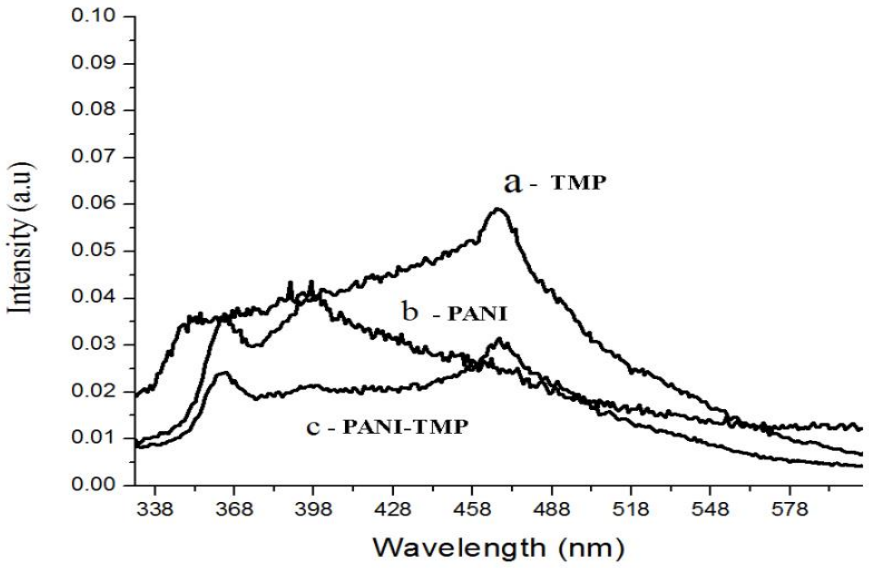

Figure 11. PL spectra of(a) TMP (b) PANI and (c) PAN /TMP

4.2.5. Scanning Electron Microscope (SEM)

Scanning electron micrographs of the different photocatalysts PANI, TMP and PANI /TMP are shown in (Fig. 12 a, b, c), respectively The elemental composition of the material was

estimated from energy dispersive X-ray equipped with scanning electron microscope. The image of PANI showed no clear morphology but porous structure making it amenable for dispersing the inorganic component. The SEM micrograph of the inorganic exchanger TMP showed aggregates of particles with no distinct morphology a closer look at the image of this exchanger with better magnification (Fig. 12b) however showed deposition of brighter spots on the surface possibly representing Sn and Mo. The SEM image of PANI /TMP composite evidences no distinct morphology making it similar to the inorganic exchanger. However, the narrow range of elemental compositions (Table 3) shown in the composite demonstrates the importance of the polymer in bringing about uniform distribution of the inorganic exchanger in the polymer matrix (Fig. 12c) .The EDX spectra of the composite exchanger evidences the binding of polyaniline with TMP in PANI/TMP nanocomposite ion exchanger (Deepak *et al.*, 2014).

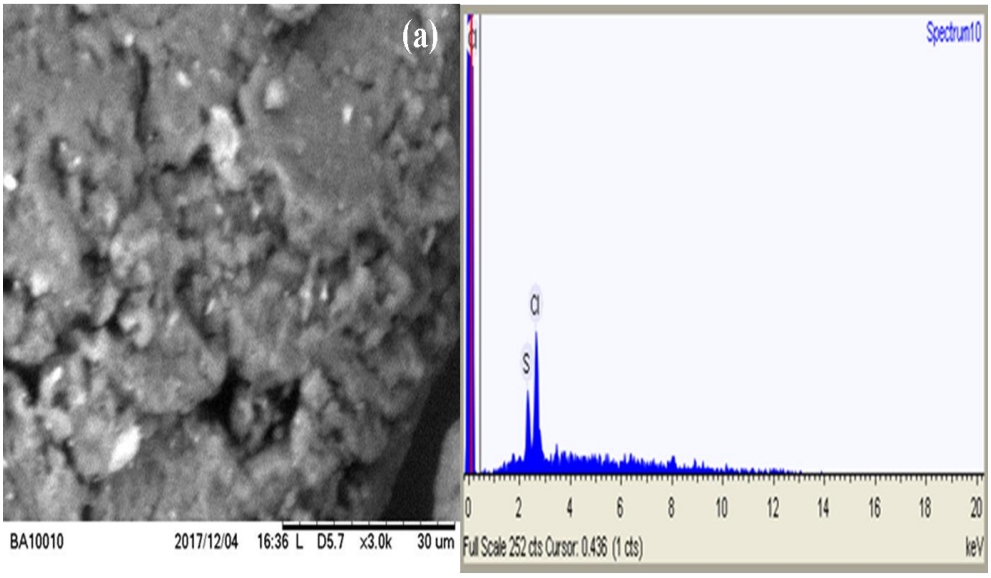

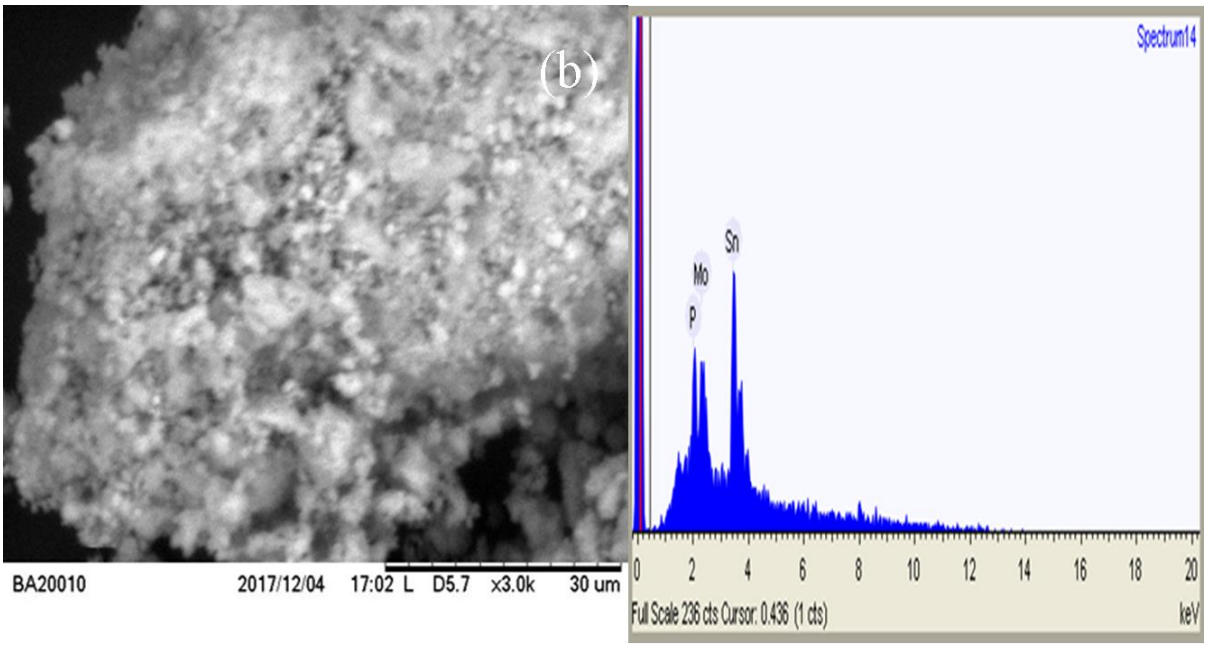

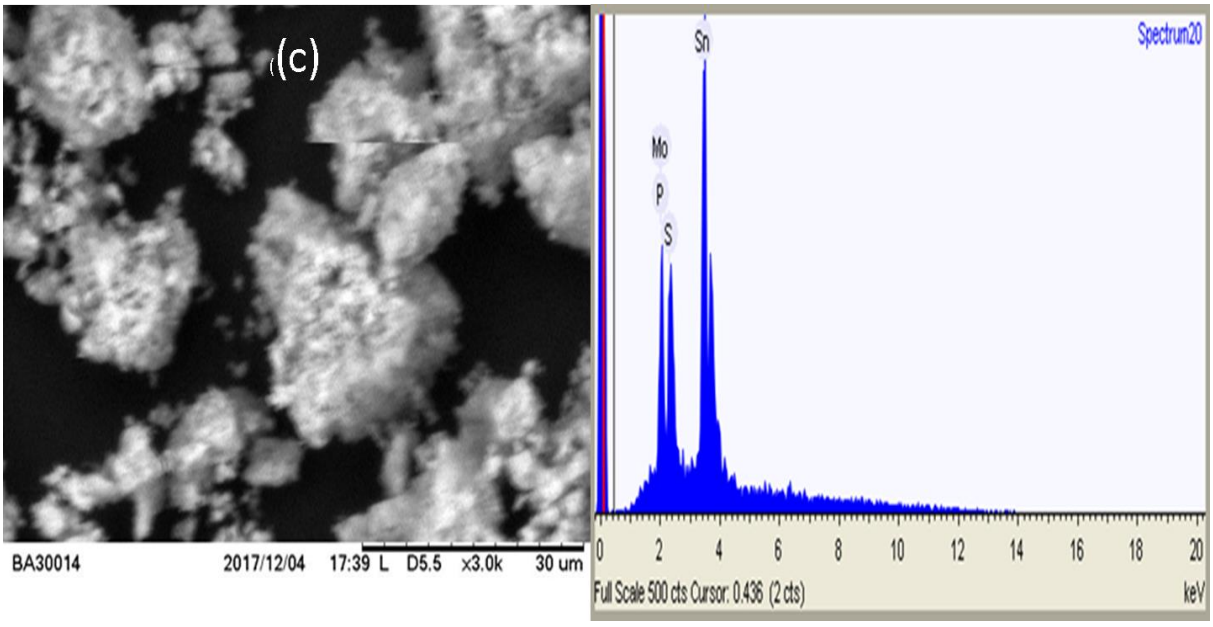

Figure 12. SEM-EDX image of (a) PANI, (b) TMP and (C) PANI/TMP

Table 3. Elemental composition of PANI, TMP and PANI/TMP

Element	Weight % in range			Weight % in average		
	PANI	TMP	PANI/ TMP	PANI	TMP	PANI/ TMP
Sulfur	25-25.9		0.7 - 3.3	25.45		1.83
Chlorine	74.1-75.0			74.55		
phosphorus		8..0 – 12.2	8.7 -10.3		9.91	9.65
Molybdenum		17.5 – 34.7	15.6 -17.7		21.57	16.4
Tin		57.3 – 72.3	70.6 -75.0		68.43	72.25

4.3. Photocatalytic Degradetion study

The photocatalytic degradation performances of photocatalysts; TMP, PANI and PANI / TMP in the degradation of MB were evaluated using initial dye concentration of 10 ppm and the catalyst load of 100 mg/L under visible light radiation for a period of 180 min. The characteristic absorptions of MB at λ_{max} 665 nm were employed to monitor the photocatalytic degradation process. The degradation efficiency of methylene blue was calculated from the reaction profiles in (Fig. 14) using the simple equations as follows:

$$\% \text{ Degradation} = 1 - \frac{C_t}{C_o} \times 100 \qquad (11)$$

Where: C_o is the initial concentration and C_t is the concentration of MB at different irradiation times.

The percentage degradation of methylene blue under visible light irradiations using TMP, PANI and PANI/TMP was found to be 26.4, 34.9 and 60.1%, respectively as demonstrated in (Fig.14) and Appendix Table 4. The rate of photocatalytic degradation of PANI/TMP composite was higher than PANI and TMP this is due to coupling of PANI and TMP in the composite.

Generally, the rate of photocatalytic degradation of TMP < PANI < PANI /TMP under visible light irradiation and the highest rate photocatalytic degradation which is PANI-Sn (IV) molybdophsphate and it was selected for the subsequent experiments.

The band gap energy (E_g) of Sn (IV) molybdophosphate is about 3.1 eV, corresponding to a threshold wavelength of 210 nm. The weak degradation of the methylene blue dye in pure Sn (IV) molybdophosphate is due to the poor light absorption under visible irradiation. For photocatalytic behavior under visible-light irradiation, the introduction of PANI to Sn (IV) molybdophosphate nanoparticles obviously enhanced the photo activity. PANI has a narrower band gap, showing strong absorption in the range from visible to near infrared light (Sandhya and Sugunan, 2014). Hence, it may function as an effective sensitizer to Sn(IV) molybdo phosphate photocatalysts. Based on energy band theory of PANI- Sn(IV) molybdophsphate composites, the photocatalytic mechanism under visible light irradiation is described in (Fig. 13).

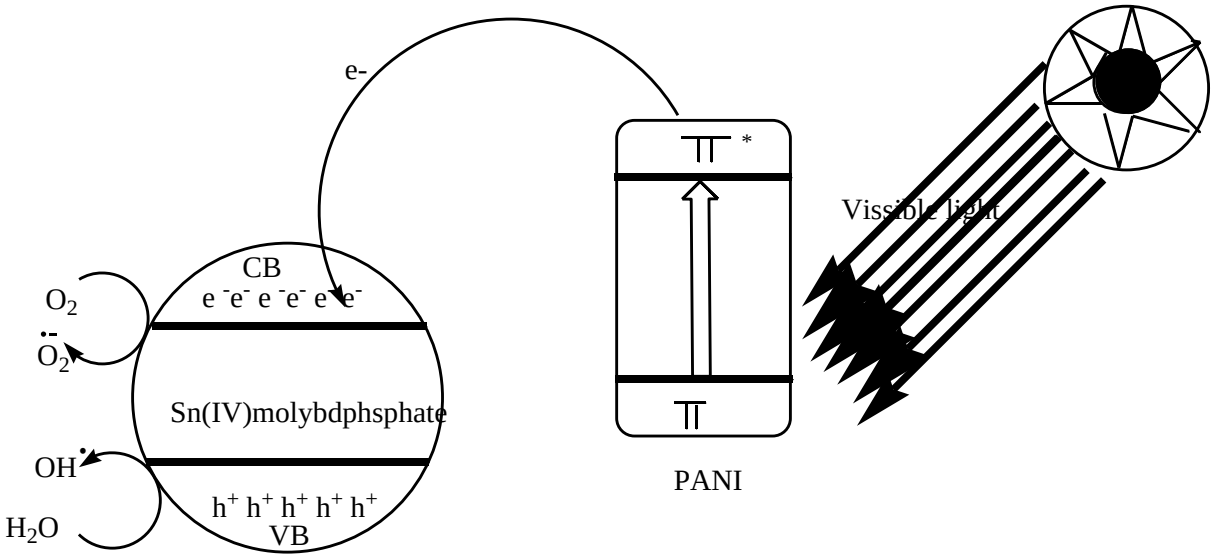

Figure 13. Mechanism of photocatalytic degradation of dyes using PANI /TMP

It is well known that the overall photocatalytic activity of photocatalyst is mainly governed by three properties: light harvest efficiency, separation efficiency of photo generated charges and the interfacial reaction process. The high separation efficiency of photo generated charges could be achieved by the hetero junction built between Sn(IV) molybdophsphate and PANI.

The energy levels of PANI have been known as well-matched for wide band gap semiconductor Sn(IV) molybdophsphate. Both PANI and Sn (IV) molybdophsphate nanoparticles absorb photons at their interface under irradiation. Since the CB of Sn(IV) molybdophsphate and lowest unoccupied molecular orbital (LUMO) of PANI are well matched for the charge transfer, the electrons generated by PANI $\pi \rightarrow \pi^*$ transition under visible light illumination can be injected into the CB of Sn(IV) molybdophsphate and the electrons in the VB of Sn(IV)molybdophsphate are delivered to PANI layer. In consequence, the enhancement of charge separation in the PANI - Sn(IV) molybdophsphate nanocomposite can be achieved very easily because PANI is an efficient electron donor and a good hole transporter as well. These features of PANI lead to the effective separation of photo generated electron–holes at the interface of PANI and Sn (IV) molybdophsphate in the nanocomposite.

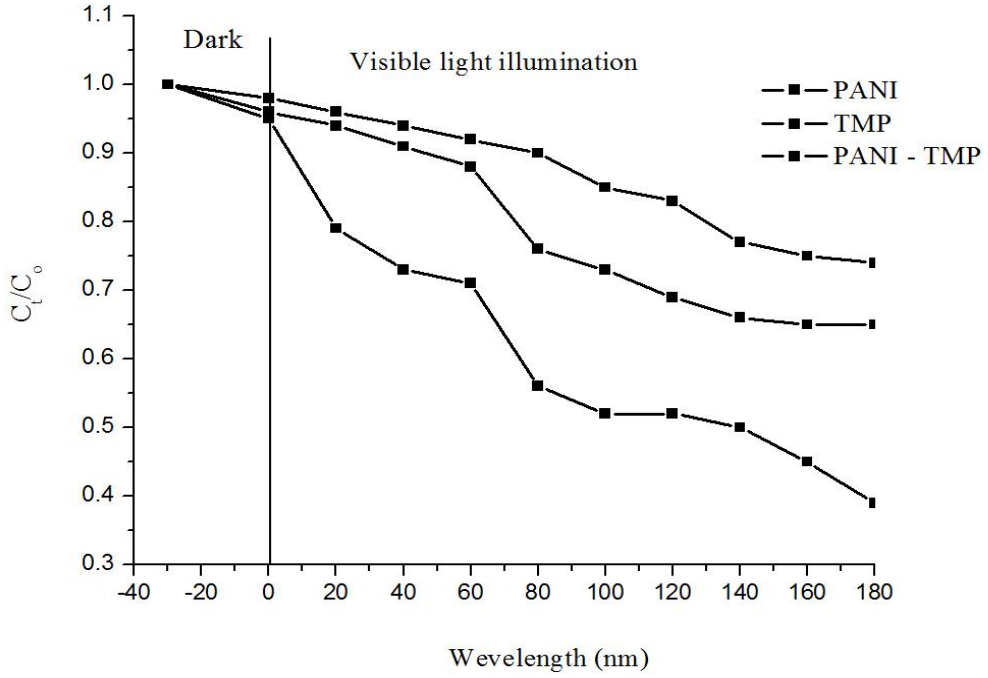

Figure 14. Plot of C_o/C_t versus time for photpcatalytic degradation of MB using PANI, TMP and PANI/TMP photocatalysts under visible irradiation Dye initial concentration 10 ppm, photo catalyst lode 100 mg L^{-1} without pH adjustment.

4.4. Effect of operational parameter on photocatalytic degradation of MB

4.4.1. Effect of the Solution pH

The pH can affect the catalyst-pollutant interactions and generation of redox species during irradiation (Tang *et al*., 1997). Photocatalyst surface is predominantly negatively charged when the pH is increased beyond the isoelectric point of a photocatalyst. As the pH decreases, the functional groups are protonated, thus raising the positive charge on the photocatalyst surface. On the other hand the surface of photocatalyst would be charged negatively at higher pH and this result in the increased adsorption of cationic molecules, while in the reverse situation it would adsorb anionic molecules very easily (Rajabi *et al.,* 2013). In the meantime, the increased pH value increases the hydroxyl radical's generation (Chiang and Lin, 2013). But the degradation of organic molecules is repressed when the pH of solution is too high (pH > 12), because hydroxyl ions compete with organic molecules for the adsorption on the surface of the catalysts (Rajabi *et al*., 2013). On the contrary, at low pH, the adsorption of cationic organic molecule on the photocatalyst surface is reduced, because the surface of photocatalyst is positively charged which results in the decrease in adsorption of cationic organic molecules. The effect of pH on the degradation of MB can also be explained in similar way to the above. In addition, in the photocatalytic process, the number of photo generated electrons and holes that reach the surface of the particles determines the efficiency of the dye's degradation (Yao *et al*., 2004).

To examine the pH effect, a serious of experiments were conducted at pH 2, 4, 6, 8, 10 and 12 with initial dye concentration of 10 ppm and catalyst load of 100 mg/L as a function of irradiation time of 180 min. The result of this study is depicted in Figure 14 and Appendix Table 5. The phtodegradation of MB is found to be 32.4%, 37.5%, 46.4%, 72.9%, 51.2% and 48.5 % at pH 2, 4, 6, 8, 10, 12 respectively. These results show that the MB phtodegradation efficiency was increased from 32.4 % (pH=2) to 72.9 % (pH= 8) and decreased to 48.5 % when pH is increased to 12. This indicates the degradation efficiency is higher in basic than acidic conditions. Because MB is a cationic dye, its structure becomes positively charged when it is dissolved in water.

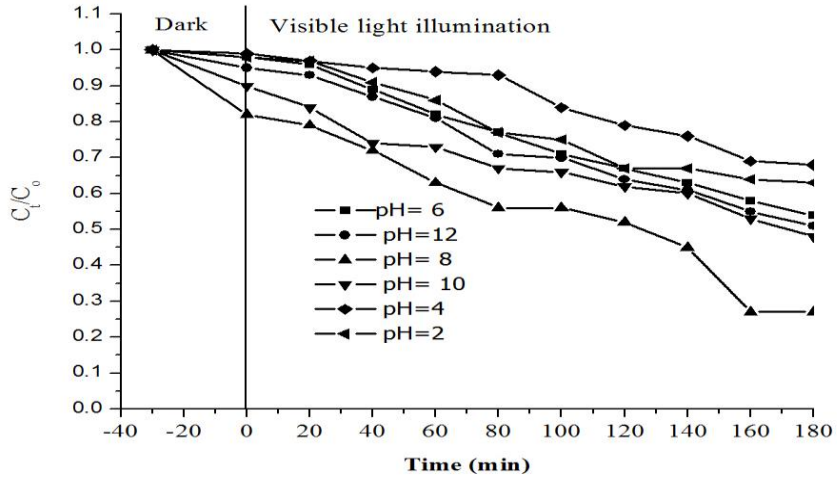

Figure 15. Plot of C_o/C_t versus time for photocatalytic degradation of MB using and PANI /TMP photocatalysts under visible irradiation dye initial concentration (10ppm), photocatalyst load (100 mgL^{-1}) and at different pH

The phtodegradation increased considerably with an increase in pH since the surface of the particles is negatively charged when the solution pH is higher than the zero point charge pzc (5.09). These opposite charges between the solution and the surface of the particles enhanced the degradation of MB. Therefore, we believed that the increase in the degradation rate at higher pH value can be explained as a higher pH value could provide a higher concentration of hydroxyl ions that can react with the photogenerated holes to form $OH^{-\cdot}$and subsequently enhance the degradation of MB. On other hand, the surface of MB is positively charged; the photogenerated electrons can transfer to the surface of the particle and enter the molecular structure of MB which leads to the decomposition of MB (Qi *et al*., 2008; Qi *et al*., 2009). In acidic or neutral pH medium the degradation rate of MB decreased because it cannot provides enough hydroxyl groups to form $OH^{-\cdot}$. Besides, at lower pH, the photocatalyst would develop positive charge. As the dye is a cationic one, electrostatic repulsion would prevail which in turn is the reason for reduced interaction between the dye and the surface of the photocatalyst which lead to decreased photo catalytic efficiency. The photocatalyst exhibiting maximum rate of degradation (72.9 %) at pH = 8 at 180 min, this was selected as optimum pH in the subsequent experiments. Unlike others, the percent degradation declined beyond this time. The

general trend is, however, similar to previous studies done on similar photo catalytic degradation reactions.

4.4.2. Catalyst Loading

The experiment was conducted by varying the concentration of as synthesized selected polyaniline tin (IV) molybdophosphate photocatalyst keeping pH at 8, dye concentration at 10 ppm and irradiation time of 180 min. The photocatalyst load was ranged from 10 mg/L to 400 mg/L. The results of this experiment are shown in (Fig. 15) and Appendix Table 4. Accordingly, the phtodegradation efficiency increased from 10 mg/L to 100 mg/L and further increase of catalyst loading from 100mg/L to 400mg/L results in decreasing degradation of MB. This observation may be explained in terms of restricted active sites on photocatalyst surface. Furthermore, it was reported that for a very high particle concentration the suspension turbidity increases. In this situation, the visible light penetration decreases, as a result of an enhanced visible light scattering effect, and consequently the photocatalytic degradation becomes less effective (Mohammad *et al*., 2015). At the time at lower photocatalyst loading, the degradation of organic molecule (MB) was low, because more light is transmitted through the reactor and lesser transmitted radiation only will be utilized in the photo catalytic reaction (Neppolian *et al*., 2002). The tradeoff between these two opposing phenomena results in an optimum catalyst loading for the photo catalytic reaction (Adesina, 2004). The optimum catalyst dose for synthesized nano-composite was 100mg/L. The result was similar to (Pathani *et al*., 2013). A catalyst load of 100 mg/L.is therefore selected as optimum value for the subsequent experimental work.

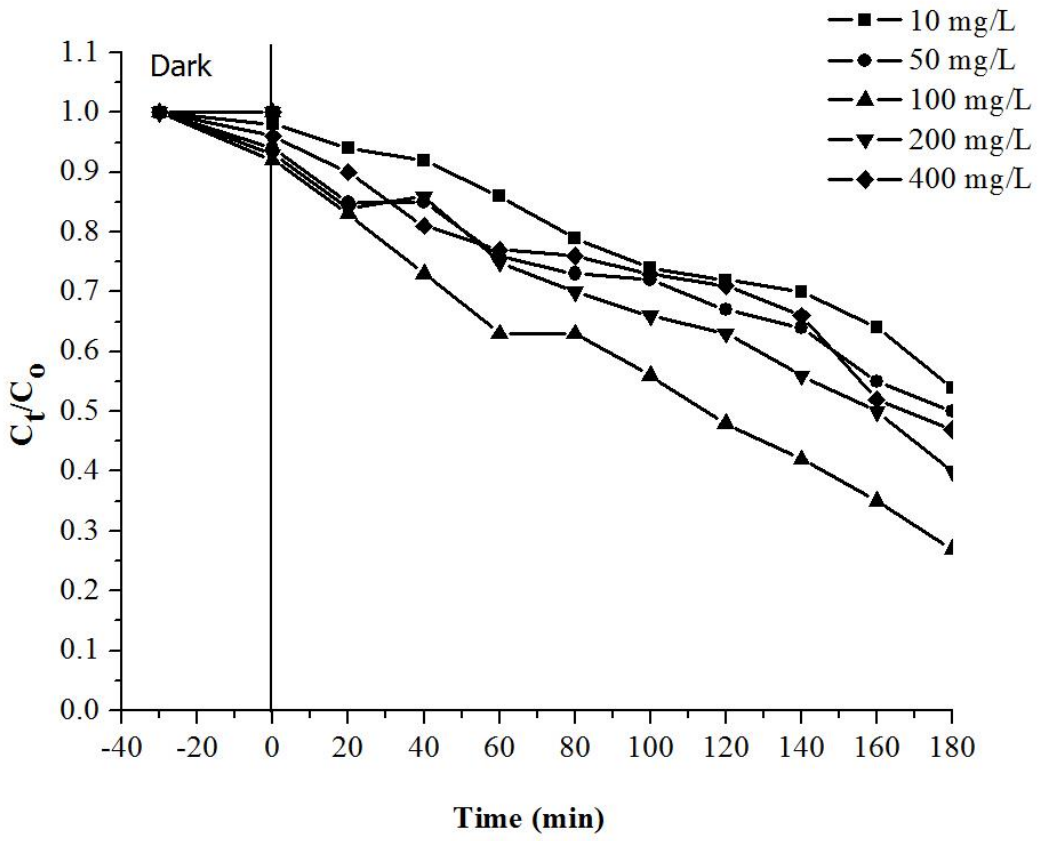

Figure 16. Plot of Co/Ct versus time for photpcatalytic degradation of MB using and PANI /TMP photocatalysts under visible irradiation Dye initial concentration (10 ppm), at PH (8) and different photocatalyst load.

4.4.3. Effect of Dye concentration in Photocatalytic Activities

The effect of initial dye concentration on the photocatalytic degradation efficiency was studied in the concentration range from 10 mg/L to 30 mg/L of MB solution. The other parameters such as catalyst dose and pH were kept at 100 mg/L and 8 respectively. The experimental results showed that; the rate of degradation efficiency decreased when the concentration of MB increased from 10 to 30 mg/L, which is from 73 % to 39 % upon 180 min visible light irradiation (Fig.17 and Appendix Table 5) This may be due to increased dye molecules around the photocatalyst with a constant (fixed) active cites that causes prevention of the visible light penetration from striking the surface of the photocatalyst. This effect resulted in the reduction

of the photo generation of relative amount of holes or $^{\bullet}OH$ and $^{\bullet}O_2^-$ on the surface of the catalyst with the intensity of light and irradiation time and hence degradation rate decreases (Haileyesus *et al*., 2015). Generally, as the dye concentration increases they covered the active cites of the photocatalyst surface which decreases the photo generation of holes or •OH that in turn decreases the photodegradation of MO and additionally the dye ions may absorb significant amount of visible light rather than the PANI/TMP particles and reduces the efficiency of photocatalytic reaction. Thus, the optimum amount of MB at which its degradation rate is highest was found to be 10 mg/L.

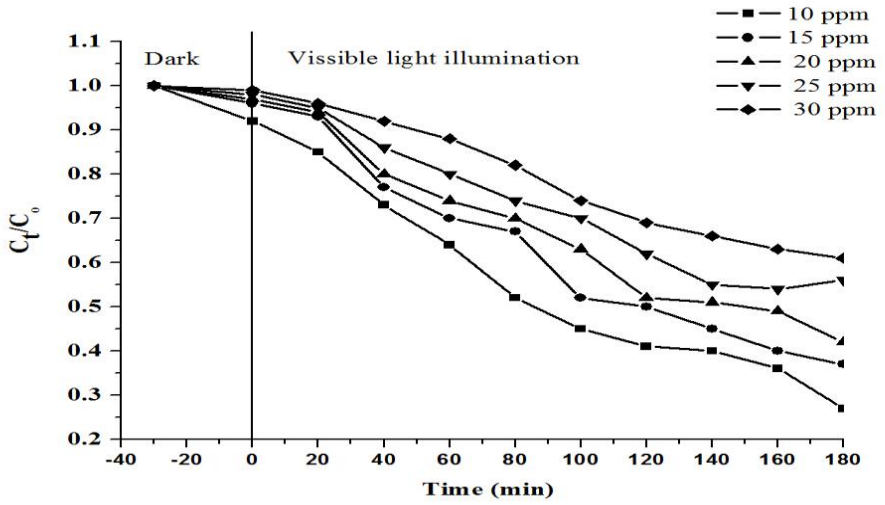

Figure 17. Plot of C_t/C_o versus time for phtodegradation of MB dye under visible irradiation using PANI/TMP photocatalyst at different initial dye concentration.

4.4.4. Mechanism of Scavenger Reaction

To evaluate the mechanism of photocatalytic degradation of polyaniline Tin(IV) molybdophosphate nanocomposite (PANI TMP) over methylene blue, the influences of active species such as superoxide radical $^{\bullet}O_2^-$ hole (h^+)and hydroxyl radical ($^{\bullet}OH$) in the photo degradation process were evaluated using 10 ppm of MB and 100 mg/L of the photocatalyst at pH = 8. Different scavengers were used to remove the corresponding active species so that the function of different active species in the photocatalytic activities process based on the change of photocatalytic conversion of targeted pollutant methyl blue could be understood.

The scavengers used in this reaction were $NaHCO_3$ for h^+, CH_3OH/H_2O for $^{\bullet}OH$ and $AgNO_3$ for superoxide radical $^{\bullet}O_2^-$ (Qamar *et al*., 2005; Liu *et al*., 2013) (Fig. 18).

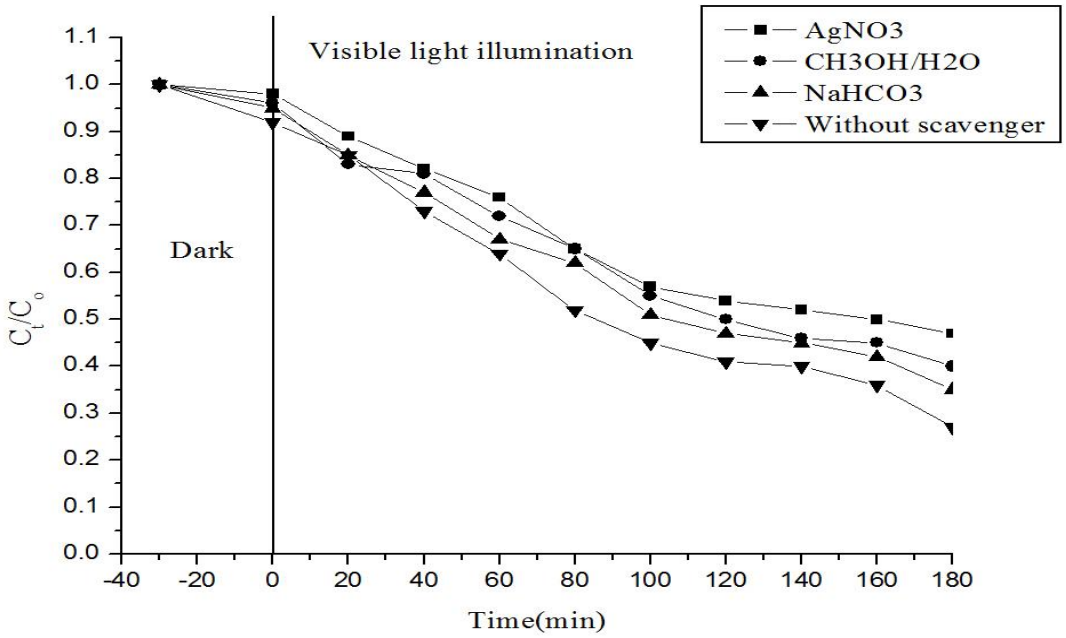

Figure 18. Plot C_t/C_o MB as function of time in presence of different scavenges

The photocatalytic conversion of MB without scavenger was 72.96%. When $AgNO_3$ was added, the photocatalytic degradation of MB decreased to 53% whereas when CH_3OH/H_2O and $NaHCO_3$ were added, the photocatalytic conversion of MB become 60% and 67.5% respectively. The results indicated that all the scavengers considered have suppressed the photocatalytic degradation efficiency although the effect of $AgNO_3$ and CH_3OH/H_2O are more pronounced. Therefore, the main active species in this photodegradation reaction is superoxide radical $^{\bullet}O_2^-$ and hydroxyl radicals. The direct involvement of holes appeared to be restricted. Rather the holes involve indirectly via the reaction of these species with water molecules to create a very reactive hydroxyl radicals. This experiment evidences the involvement of the conduction band electrons and the valence band holes in the redox process corroborating the highest photocatalytic efficiency of the organic-inorganic composite compared to their organic and inorganic counterparts.

4.5. Kinetic Study of Photocatalysts

The kinetics of photodegradation of MB with polyaniline-Tin(IV) molybdophosphate nanocomposite (PANI /TMP) in visible light is demonstrated in Figure 18 where the plots of ln (C_0/C_t) versus irradiation time are shown for MB. We can see that the degradation process follow pseudo first order kinetics when the plot gives straight line of slope k using the simple equations as follows:

$$\ln (C_0/C_t) = k\, t \qquad (12)$$

Where, C_t is the concentration of dye after irradiation and C_o is the concentration after the adsorption equilibrium on the photocatalyst particles before irradiation, K is pseudo first order rate constant and t is irradiation time.

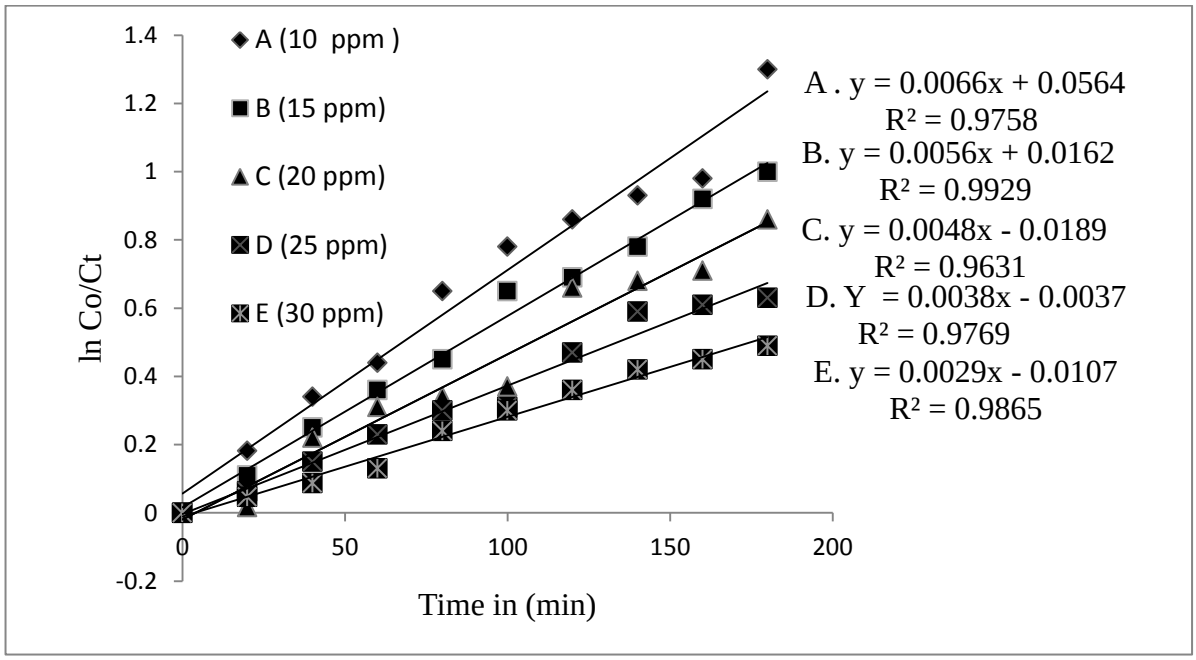

Figure 19. Plot of ln Co/Ct versus time for photo degradation of MB dye under visible irradiation using PANI/TMP photocatalyst at different initial dye concentration.

The values of ln (C_o/C_t) as a function of *t* are presented in (Appendix Table 7) and their corresponding plots in (Figure 18). From the linear correlation of the plot, it suggested that MB dye is a pseudo first order kinetics. Rate constant using different dye concentration using

photocatalysts are $0.7x10^{-3}$ min^{-1}, $5.7x10^{-3}$ min^{-1}, $4.7x10^{-3}$ min^{-1} , $3.7x10^{-3}$ min^{-1}, $2.8x10^{-3}min^{-}$ respectively and the correlation constant R^2 for the fitted line was calculated to be 0.9758,0.9929, 0.9969, 0.9631, and 0.9865 for MB concentration of 10, 15, 20, 25 and 30 mg/L, respectively. Fairly good correlation to the pseudo first order reaction kinetics (R^2 > 0.9929) was found.

4.6. Antimicrobial Activities of as-Synthesized Nanocomposite

It has been revealed that maximum inhibition of *Salmonella typhus* and *Staphylococcus aureus* was at 0.01g/mL PANI/TMP. The death phase was observed after 24 h incubation. The antimicrobial activity of PANI, TMP and PANI /TMP was checked for same concentration i.e.,0.01g/Ml by disc diffusion method. The antimicrobial efficiency of as synthesized Nanomaterial polyaniline, Tin(IV) molybdophosphate, Polyaniline tin (IV) molybdophosphate were evaluated using Gram-negative (*Escherichia coli, Salmonella typhus*) and Gram-positive (*Streptococcus, Staphylococcus aurous*) bacteria by using disk diffusion method. Antibacterial activity was calculated in terms of zone of inhibition (measured in mm).We have checked the effect of the as-synthesized nano materials. In this case, almost all the nanocomposites have showed inhibition on the studied bacteria to a different extent.

Table 4. Average inhibitory effects of composite materials PANI, TMP, PANI/ TMP, DMSO and Chlorampanicol on microorganisms

Formation diagonal circulars				
	Gram-positive		Gram-negative	
	Staphylococcus a.	*Streptococcus*	*E.Coli*	*Salmonella typ.*
1.TMP	3.83 ± 0.57	5.33 ± 0.58	0	0.35 ±0 .20
2. PANI	13.5 ± 0.63	15 ± 1.70	8.66 ±0.58	17 ± 1.70
3. PANI-TMP	23.3 ± 0.63	22.33 ±2.9	10.3 ± 0.87	24.7 ± 1.75
4. DMSO	0	0	0	0
5. Chlorampanicol	38 ± 0.62	40.5 ± 1.7	27.8 ±1.26	36.5 ± 0.86

Values are mean ±S.D of samples analyzed individually in triplicate. Concentration: 0.01g/mL in DMSO, Standard: Chlorampanicol 0: no activity 5–10: activity present, 11–25: moderate activity, 26–40: strong activity.

As it can be seen from (Fig. 20) the performance of the nanocomposites in general is relatively low as compared to the reference drug, Chloramphenicol. Within the nanocomposite themselves, in general, the nanocomposite have shown to relatively greater inhibition for Salmonella typhus and staphylococcus aurous as compared to *E.Coli* and *Streptococcus*. Furthermore, the order of inactivation follow Polyaniline tin (IV) molybdophosphate > Polyaniline > Tin (IV) molybdophosphate. The results revealed the potential antibacterial activity of PANI TMP composite against microbes. The presence of material in suspension resulted in continuous release of ions into nutrient media and cross the cell membrane without hindrance and deposit over the cell organelles, impairing the intracellular transport and nutrient uptake. The nanoparticles suspension diffuses through the matrix of the agar in a circular formation. The bacteria start growing over the circle, interact with the nanoparticles, which inhibits the growth of the bacteria (Rathore *et al*., 2013).

This may be due to the binding of nanocomposite particles to the outer membrane of bacteria which resulted in the inhibition of active transport, dehydrogenase and periplasmic enzyme activities. These composite also interfere in the respiration process of the cell and therefore block the synthesis of proteins, which restricts further growth of the pathogens (Saddiqui *et al*., 2007).The results of average inhibition zone of PANI, TMP, PANI/TMP, DMSO and Chlorampanicol on different bacteria were shown in Table 4.

Figure 20. A schematic illustration of created inhibition zones for antibacterial activity of 1.TMP, 2. PANI, 3. PANI/TMP, 4. DMSO 5. Chlorampanicol

5. SUMMARY, CONCLUSIONS AND RECOMMENDATIONS

5.1. Summary and Conclusion

Polyaniline was prepared by mixing 10 % (v/v) aniline and 0.1 M ammonium peroxo-di-sulfate $(NH_4)_2S_2O_8$ in 1M HCl. Inorganic nanocomposite Tin (IV) molybdophosphate was synthesized by mixing equal volumes of the solutions of $SnCl_4$. $5H_2O$ (0.2M), H_3PO_4 (0.1 M) and Na_2MoO_4 $2H_2O$.(0.1 M). Polyaniline Tin(IV) Molybdophosphate was synthesized via sol –gel method. The gel of polyaniline was added into the inorganic precipitate of tin (IV) molybdophosphate and mixed thoroughly with constant stirring for 1 h. The crystal structures, band gap energy, bond vibration (stretching), optical properties, morphologies and particle sizes of all the as synthesized photocatalysts were performed using X-ray diffraction XRD, Uv-Vis, FTIR, PL and SEM techniques respectively. Photocatalytic as well as antimicrobial activities of the as synthesized organic, inorganic and organic-inorganic nanocomposite were investigated on the target pollutant methylene blue and on the various Gram negative and Gram positive bacteria under visible irradiation. All the results confirmed that the photocatalytic as well as antibacterial activities of organic-inorganic nanocomposite Polyaniline Tin (IV) molybdophosphate was higher than polyaniline and Tin (IV) molybdopho sphate.

5.2. Recommendations

PANI-TMP nanocomposite synthesis, characterization, photocatalytic and antimicrobial applications were reported in this work. Therefore, the author recommended other researchers to pay attention for advancing further research on the following areas.

- To investigate the application of PANI/TMP on other dyes
- Looking for other polymeric or inorganic supports to immobilize TMP to enhance the efficiency, attempt potential application in the area of sensors, solar cells, super capacitors, fuel cells etc.
- Involve photocatalytic parameters on antibacterial activity, such as the influence of time, effect of amount of catalyst, and effect of light intensity

- ☞ cytotoxic effects and the bactericidal effects of PANI-TMP nano composites against different types of bacteria for potential widening of their applications, such as in surgical devices and in drug-delivery are among many other important factors that should be given equal attention to increase the efficiency.

6. REFERENCES

Acharya, A., Mishra, R. and .Roy, G.S. 2010. Comparative study of performance of CdS, CdSe thin film CdS-PTh, CdSe-PTh nanocomposite thin films using SEM-EDXA and FTIR. *Latin-American journal of Physics education*, 4(3): 177–185.

Adesina. 2004. Industrial exploitation of photocatalysis: progress, perspectives and prospects. *Catalysis Surveys from Asia*, 8(4): 265-273.

Ahmed, S., Rasual, M.G., Brown, R. and Hashib, M. A. 2010. Influence of parameters on the photocatalytic degradation of pesticides and phenol contaminants in waste water. *Journal of Environmental Management*, 9: 311-330.

Aksu, Z. 2005. Application of bio sorption for the removal of organic pollutants: A review, *Process Biochemistry*, 40: 997-100.

Altaher, A. and ElQada. E. 2011. Nano composite pectin Zr (IV) selenotungstophosphate. *International Journal of Energy and Environment Engineering*, 211:13–24.

Anbia, M. and A. Ghaffari. 2011. Removal of malachite green from dye wastewater using mesoporous carbon adsorbent. *Journal of. Iranian Chemical Society*, 8: 67-76.

Asahara and Koseki, H. 2009. Bacterial performance of photocatalytic titanium dioxide particle mixture under ultraviolet and fluorescent light. *Surface Interface Analysis*, 41: 771-774.

Bahnemann, W., Muneer, M. and Haque .M.M. 2007. Titanium dioxide – mediated photocatalysed degradation of few selected organic pollutants in aqueous suspensions. *Catalysis Today*, 124: 133-148.

Bamlaku Semegn., Isabel, Diaz., Tesfahun Kebede .and Abi Tadesse. 2016. Synthesis, characterization and analytical application of polyaniline tin(IV) molybdophosphate composite with nano crystalline domains. *Reactive and Functional Polymers*, 98: 17-23.

Barka. N, Assabbane. A., Nounah. A., Laanab. L., Ichou, Y. 2009. Removal of textile dyes from aqueous solutions by natural phosphate as a new adsorbent. *Desalination*, 235:264.

Bera, D., Qian, L., Tseng, T.K. and Paul H. 2010. Holloway Quantum Dots and their multimodal applications**:** *Review Materials, 3*: 2260-2345.

Bharti, S. K. and Varshney. 2010. Analysis of the impact of a uracil DNA glycosylase attenuated in AP-DNA binding in maintenance of the genomic integrity in Escherichia coli. *Nucleic Acids Research,* 38 (7): 2291-2301.

Bootz, A., Vogel, V., Schubert, D. and Kreuter, J. 2004. Comparison of scanning electron microscopy, dynamic light scattering and analytical ultracentrifugation for the sizing of poly (butyl cyanoacrylate) nanoparticles. *European Journal of Pharmaceutics and Biopharmaceutics*, 57: 369-75.

Bushra, R., Naushad, M., Adnan, R., Alothman, Z.A.and Rafatullah, M. 2015. Polyaniline supported nano composite cation exchanger: synthesis, characterization and applications for the efficient removal of Pb^{2+} ion from aqueous medium .*Journal of Industrial and Engineering Chemistry*, 21: 1112–1118.

Cao, J., Luo, B.D., Lin, H.L., Xu and B., Chen, S. 2012. Aluminum salt slag characterization by nano zero-talent iron immobilized in mesoporous silica microspheres. *Journal of Hazardous Materials*, 193:70–81

Caruso, M. 2001. Antoinette, Sol-gel nano coating: an approach to the preparation of structured materials. *Chemistry of Materials*, 13(10): 3272–3282.

Chen, C. Z and Zhou, Z.W. 2007. Preparation of nano ZnO and its middle Infrared ultraviolet visible light absorption properties. *Journal of Functional Materials*. 35(1):97-98

Chiang, Y. and Lin, C. 2013. "Photocatalytic decolonization of methylene blue in aqueous solutions using coupled ZnO/SnO_2photocatalysts." *Powder Technology*, 246: 137–143.

Chira, R., Bhattacharjee, D. and Abhijit, N. 2011. *Physical Science Technology*, 7: 122.

Ciric-Marjanovic, G. 2013. Recent advances in polyaniline composites with metals, metalloids and nonmetal. *Synthetic Metals*, 170:31–56.

Debasis, B. Qian, Kuan, T. Tseng and Holloway, P.H. 2010. Quantum Dots and Their Multimodal Applications: A Review. *Materials*, 3(4), 2260-2345.

Deepak, P., Gaurav .S. Amit, K. and .Kothiyal, N.C .2014. Fabrication of Nanocomposite Polyaniline Zirconium (I V) Silicophosphate for Photocatalytic and Ant i-bacterial Activity. *Journal of Alloys and compounds. Doi*.10:1016

Dhar, S. 2007. Formation, dynamics, and characterization of nanostructures by ion beam irradiation. *Critical Reviews in Solid State and Materials Sciences*, 32(1): 1–50.

Ece, 2012. Modern methods for rapid X-ray diffraction data collection from crystals of electrode. Nature, 238: 37-38.

El-Kemary, M., H.El-shamy and I.El-mahasseb, 2010. Photocatalytic degradation of Ciprofloxacin drug in water using ZnO nanoparticles. *Journal of lamination*, 130:2327-2331.

Escobedo, A.M., Sanchez, E.M. and Pal, U. 2007. Use of diffuse reflectance spectroscopy for optical characterization of unsupported nanostructures. *Journal of Optical Materials*, 53(5): 18-22.

Fan. L.Y., Yang. W., Chen, G. and Yang, F. 2008. Removal of Methylene Blue, Rhodamine B and Ammonium Ion from Aqueous Solution by Adsorption onto Sintering Porous Materials Prepared from Coconut Husk Waste. *Open Journal of Inorganic Non Metallic Materials*, 76: 440–446.

Fischer, V.I., Lieberwirth. G., Jakob R., Fester, L. and Munoz-EspiAta, 1999. *Journal of current chemistry.* 2:189-196.

Fox M. A. and Dulay1 M. T. 1993. Heterogeneous Photocatalysis . *Chemical Reviews*, 93(1): 341-357.

Fujishima, A., Rao, T.N, Tryk, D.A., 2000. Titanium dioxide photocatalysis. *Journal of Photochemistry and Photobiology*. C: Photochemistry. Review. 1: 1–21.

Fujishima, A. and Honda, K. 1972. Electrochemical photolysis of water at a semiconductor Electrode. *Nature*, 238: 37-38.

Gupta V. K., Pathania. P., Singh. D., Rathore. P. and Chauhan. 2013. Fabrication of nano composite polyaniline zirconium (IV) silicophosphate for photocatalytic and antimicrobial activity, *Journal of Alloys and Compounds Polymer* , 95: 434–440.

Gupta, V. K., D. Pathania, P. Singh, A. Kumar and Rathore .B. S. 2014 Adsorption removal of methylene blue by gaur gum - cerium (IV) tungstate hybrid cation exchanger. *Carbon. Polymer*.101: 684-691.

Gupta, V.K., Agarwal, S., Pathania, N.C., Kothiyal, G. and Sharma, C.2013. Use of pectin – thorium (IV) tungstomolybdate nanocomposite for photocatalytic degradation of methylene blue. *Carbohydrate Polymer*, 96: 277–283.

Hager, T. 2006. Battlefield Hospitals to Nazi Labs, One Doctorís Heroic Search for the World is First Miracle Drug. *Crown Publishing Group*, New York.

Haileyesus, Tedla. Isabel, Diaz. Tesfahun, Kebede. Abi M, Taddesse. 2015. Synthesis, Characterization and photocatalytic activity of zeolite supported $ZnO/Fe_2O_3/MnO_2$ nanocomposite. *Journal of Environmental Chemical Engineering*, 3: 1586–1591.

Herrman, J.M. 1999. Heterogeneous photocatalysts: fundamentals and applications to the removal of various types of aqueous pollutants. *Catalysis Today*, 53:115-129.

Hoffmann, M. R. Martin, S., Choi, W.Y. and Bahnemann, D.W. 1995. Environmental Applica tions of Semiconductor Photocatalysts. *Chem Rev*iew, 95: 69-96.

Hoffmann,.M.R.,Martin, S.T., Choi, W. and Bahnemann, D.W. 1995. Environmental applications, *Journal of international energy environmental engineering*, 211: 13–24.

Hong, R.Y., Li, J.H., Chen, L.L., Liu, D.Q., Li, H.Z., Zheng, Y. and Ding, J. 2009. Synthesis, surface modification and photocatalytic property of ZnO nanoparticles. *Journal of Powder Technology*, 189: 426-432.

Ibezim, 2005. Microbial resistance to antibiotics. *African Journal of Biotechnology*, 4(13): 606-611.

Jianyong, O., Chih. - Wei, C., Ricky, J., Ankitha, P., and Yang. 2006. Hand Book of conducting polymers. 3rd Edition. *Processing and applications*.

Kamat, P.1993. Photo physical, photo chemical and photo catalytic aspects of metal nanoparticles. *Chemical Engineering Review*, (93): 267-300.

Kamigaito, O., Moore, D.R., Sato, N., Kurauchi, T. and Sato, S.1991. Fatigue of thermoplastic composites, in thermoplastic technology and engineering. *Journal of Materials Science, 26*: 3891-3898.

Kant, S., Pathania, D., Singh, P., Dhiman, P., Kumar, A., 2014. Removal of malachite green and methylene blue by Fe0.01Ni0.01Zn0.98O/polyacrylamide nanocomposite using coupled adsorption and photocatalysis. *Applied Catalysis B: Environmental*, 147, 340-352.

Kar. S., Pal, B.N., Chaudhuri, S. and Chakravorty, D. 2006. One-dimensional ZnO monostructure ARRAYS: Synthesis and characterization. *Journal of Physical Chemistry* B.110: 4605-4611.

Katsumata, H., Hayashi, T., Taniguchi, M., Suzuki, T., Kaneco, S. 2014. Highly efficient visible light driven $AgBr/Ag_3PO_4$ hybrid photocatalysts with enhanced photocatalytic activity Materials Science in Semiconductor Processing, 25: 68–75 .

Kavitha, B., Prabakar, K., Siva kumar, K., Srinivasu, D., Srinivas, Ch., Aswal,V.K., Siriguri,V. and Narsimlu, N. 2012. Spectroscopic Studies of Nano Size Crystalline Conducting Polyaniline, *Journal of Applied Chemistry*, 2:16-19.

Khan, A. A. and Khan, A. 2010. Ion-exchange studies on poly-o-anisidine Sn (IV) phosphate nano composite and its application as Cd (II) ion-selective membrane electrode. *Central European Journal of Chemistry*, 8: 96 - 408.

Khan, A.A. and Paquiza. L. 2011. Characterization and ion-exchange behavior of thermally stable nano-composite polyaniline zirconium titanium phosphate its analytical application in separation of toxic metals, *Desalination*. 242–254.

Kickelbick, 2007 Hybrid Materials: Synthesis, Characterization, and Applications. *Journal of Materials Chemistry*, 337-400.

Klaas, J., Schulz-Ekloff, G. and Jaeger, N.I. 1997. UV-Visible diffuse reflectance spectroscopy of Zeolite-hosted mononuclear Titanium oxide species. *Journal of Physical Chemistry*, 101(8): 1305-1311.

Kose.T. D. and Ramteke, S.P. 2012. Fabrication of nano composite polyaniline zirconium (IV) silicophosphate for photocatalytic and antimicrobial activity. *International Journal of Computational and Material science,* 2: 44–47.

Lesley E.S., and Elaine. A.M. 2005. Solid State Chemistry.3rd Edition. Press Taylor & Francis press. Open University, Walton Hall, Milton Keyne.

Li, F.B., Li, X.Z., Liu, C.S. and Liu, T.X. 2007. Effect of alumina on photo catalytic activity of iron oxides for bisphenol degradation. *Journal of Hazardous Materials*, 149: 199-207.

Liu, Y.D., Fang, F.F., Chai, H. J. and Sego, F.Y. 2012. Fabrication of nano composite polyaniline zirconium (IV) silicophosphate. *Colloids Surface*, 381: 12–22.

Liu. W., Minglian W., Chunxiang X., Shifu. C and Xianliang. F. 2013. Ag3PO4/ZnO an efficient visible light sensitized composites with its application in photocatalytic degradation of Rhodamine B. *Material Bulletin*, 48:106-113.

Lu, X., Zhang, W., Wang.C. Ten-Chin and Wei, Prog.Y. 2011. One-dimensional conducting polymer nano composites Synthesis, properties and applications. *Progress in Polymer Science,* 36: 671–712.

Mehto. A., Mehto, V.R., Chauhan, J., Singh, I.B. and Pandy. R.K. 2017. Preparation and Characterization of Polyaniline/ZnO Composite Sensor .*Journal of Nano medicine Research,* 5:1-2017.

Miclescu, A. and Wiklund, L.2010. Methylene blue, an old drug with new indications. *Jurnalul Român de Anestezie Terapie intensive*, 17(1):35

Minbal. A., Rao Suhail. S. A., Amare, A. and Upadhyay, R.K. 2011. Synthesis and Anti-microbial Evaluation of 2-imino-3 (substitutearyl)-thiazolidin-4-one.*International Journal of Current Chemistry,* 2:189-196.

Mohamed, E.F., 2011. Removal of organic compounds from water by adsorption and Photocatalytic oxidation. Doctoral Dissertation. Paris, France.

Mohammad, Reza. Mostafa, Fazli.and Mohammad, Hossein. 2015. Decomposition of organic chemicals by zeolite TiO_2 nano composite supported onto low density polyethylene film under powered by solar radiation. Applied Catalysis B: Environmental, 183: 407–416.

Munnik, P., Petra, E. de Jongh, and Krijn P. *de Jong Inorganic* nanocomposite. *Journal of Environmental Chemical Engineering*, 3: 1586–1591

Nab. S.A., Shalla, H.A., Khan, M.A. and Ganie, S.A. 2007. Synthesis, characterization and analytical applications of titanium (IV) molybdosilicate: a cation ion-exchanger, Colloids Surface. A. *Physicochemical Engineering Asp,* 302: 241–250.

Obare, S.O., Meyer, G. 2004.TiO_2 has also been extensively studied for oxidative or reductive removal of organic pollutants. *Journal of Environmental Science and Health a toxic Hazard Substances Environmental Engineering*, 39 (10): 2549–821.

Pathani, D., Sharma, G., Kumar, A. and Kothiyal, N.C. 2013. Fabrication of nanocomposite polyaniline zirconium (IV) silicophosphate for photocatalytic andantimicrobial activity . *Journal of Alloys and Compounds,* 588: 668-675.

Pouretedal, H.R., Enkandari, H., Keshavarz M.H. and Semn, A. 2009 Photodegradation of dyes using nanoparticles of calcium sulfide doped with manganese, nickel and copper on nanophotocatalyst.*Acta. Chem. Solv*. 56: 353-361.

Qamar, M., Saquib, M. and Muneer, M. 2005. Titanium dioxide mediated photocatalytic degradation of two selected azo dye derivatives, chrysoidine R and acid red 29 (chromo trope 2R), in aqueous suspensions. *Desalination,* 186: 255-271

Qi, Xiao. Qitao, Zhou. Jiang, Zhang and Linli, Ouyang. 2009. Photo catalytic decolourization of methylene blue over monoclinic pyrochlore type Pb2Nb2O7under visible light irradiation. *Journal of Alloy Compound*, 468: 9–12.

Rathore, B.S., Sharma, G., Pathania, D. and Gupta ,V.K. Synthesis, characterization and antibacterial activity of cellulose acetate-tin (IV) phosphate nanocomposite, *Carbohydrate Polymer*, 103 (2013): 221–227.

Rajabi, J., Tayade, Ramchandra, G. and Kulkarni, J. 2013. Enhanced Photo catalytic Activity of TiO_2-Coated NaY and HY-Zeolites for the degradation of methylene Blue. Engineering Chemical Research, 46: 369-376..

Rosari, Saleh. Nadia, Fabian and. Djaja. 2014. UV-light photo catalytic degradation of organic dyes with Fe-doped ZnO nanoparticles. Super lattices and Microstructures, 74: 217–233.

Salma, M. H., Moafak, C. A. and Harith .I. J.2009. Optical Properties of Prepared Pure and Doped Polyaniline Salt. *Proceeding of 3rd scientific conference*, 2335- 2339

Sandhya .K.P. and.Sugunan.S.2014.Synthesis, Characterization and Applications of Hybrid Nanocomposites of TiO_2 with Conducting Polymers. Doctoral Dissertation, *Cochin University of Science and Technology*, Kerala, India.

Saquib, M. and Muneer, M. 2003.TiO_2 mediated photocatalytic degradation of triphenyl methane dye (gentian violet), in aqueous suspensions. *Dyes and Pigments*, 56: 37-49.

Siddiqui, W.A. and Khan ,S.A.2007. Synthesis, characterization and ion exchange properties of Zirconium (IV) monophosphate, a new cation exchanger. *Bulletin of material science* 30(1) : 43-49.

Sih, B.C. and Wolf. M.O. 2005. Metal nano particle conjugated polymer nano composites *Chemical Community*. 27: 3375–3384.

Silverstein, R.M. and Webster, F.X. 2002. Spectrometric identification of organic compounds, *6th edition*. Jhon Wiley and Sons, New York.

Snook. G. A and Kao.P.2011.Best Conducting - polymer-based super capacitor Devi electrodes. *Journal Power Source* .196:1–12.

Soutsas, K., Karayannis, V., Poulios,I., Riga, A., Ntampegliotis, K., Spiliotis, X. and Papapol ymerou,G. 2010. Decolonization and degradation of reactive azo dyes via heterogeneo us photocatalytic processes. *Desalination*, 250: 345-350.

Srinivas, C.H., Srinivasu, D., Kavitha, B., Narsimlu, N. and Siva Kumar, K.2012.Synthesis and Characterization of Nano Size Conducting Polyaniline. *Journal of Applied Physics*15: 2278-4861.

Sun, J. Qiao, L., Sun, S. and Wang, G.2008. Photocatalytic degradation of methyl orange on nitrogen-doped TiO_2 catalysts under visible light and sunlight irradiation. *Journal of Hazardous Materials*, 155: 312-319.

Tang, Junwang, Zhigang. Zou. and Jinhua, Ye.1997. Kinetics of MB degradation and effect of pH on the photocatalytic activity of MIn_2O_4 (M = Ca, Sr, Ba) under visible light irradiation. *Research on Chemical Intermediates*, 31: 513–519.

Tao, T., Zhu, S., Feng, T., Xia, C., Song, Y. and Yang, B. 2017. The polymeric characteristics and photoluminescence mechanism in polymer carbon dots, *Materials Today Chemistr y*, 6: 13-25.

Vatutsina, O. M., Soldatov, V., Sokolova, V. I., Johann, J., Bissen, M, and Weiss wnbacher.A. 2007. A new hybrid (polymer/inorganic) fibrous sorbent for arsenic removal from drink water. *Journal of environment management*, 9:311-330.

Wang, C. X. Wang, B.-Q. Xu, J. Zhao, B. Mai, Ping'an. Peng, G. Sheng and Fu, J .2004. Enhanced photocatalytic performance of Nano sized coupled ZnO/SnO2 photocatalysts for methyl orange degradation. *Journal of Photochemical Photobiology*, 168:47-52.

Wang, C., Y. Ao, P. Wang, S. Zhang, J. Qian and Hou, J. 2010. A simple method for large scale preparation of ZnS nano ribbon film and its photocatalytic activity for dye degradation. *Applied Surface Science*, 256: 4125–4128.

Wang,X., Yao, Z., Wang, J., Guo, W. and Li, G. 2008. Degradation of reactive brilliant red in aqueous solution by ultrasonic cavitation. *Ultrasonic Sonochemistry*, 15: 43-48.

Wang.C. and Herron.N.1996. Fabrication of nano composite polyaniline zirconium (IV) Silcophsphate. *Colloids and Surfaces* A, 27:32–634.

Wiklund. L, Basu .and S, Miclescu A.2007.Neuro- and cardio protective effects of blockade of nitric oxide action by administration of methylene blue. *Ann N Y Academics Science*, 1122: 231-244.

Xiao, Q., Zhang, J., Xiao, C., Si, Z. and Tan, X. 2008. Solar photo catalytic degradation of methylene blue in carbon-doped TiO_2 nanoparticles suspension. Solar Energy, (82):706-713.

Xu, Z. and Yu, J. 2011. Visible-light-induced photo electrochemical behaviors of Fe-modified TiO_2 nanotube arrays .*Nano scale*, 3: 3138–3144.

Yadav, P.S., Prakash, D. and Senthilkumar, G.P. 2011. Different Methods of Synthesis and Diverse Biological activities. *International Journal of Pharmaceutical Sciences and Drug Research,* 3: 01-07.

Yang, G., Q. Zhang, W., Chang and W. Yan .2013.Fabrication of Cd1-X Zn X S/ TiO_2 heterostructures with enhanced photocatalytic activity. Journal of. Alloys Compd. 580: 29-36.

Yao, W.F., Xu, X. H. Wang, H., Zhou, J.T., Yang, X.N. , Zhang, Y. , Shang, S.X. and Huang, B.B. 2004. Photocatalytic property of perovskite bismuth titanate. *Applied Catalyst, B: Environmental*. 52: 109–116.

Yavari, R., Ahmadi, S. J., Farkhondehru, K. Gholipoor, V. and Kamal. 2014. Evaluation, characterization and analytical application of a new composite material for removing metal ions from wastewater. International Journal of Environmental. Science and Technology, 11: 1073–1080.

Zhang, L. and Jimei, M. 2001. Nano phase Materials and Nanostructure. *Beijing: Science press*. 140-144.

Zhen, M and Francisco, Z, 2006. Heterogeneous Catalysis by Metals in Encyclopedia of Inorganic Chemistry, John Wiley. doi:10.1002/0470862106.ia084

Zhu, Y., Xu, S. Yi, D. 2010. Photocatalytic degradation of methyl orange using polythiophene titanium dioxide composites: Reactive & Functional Polymers, 70: 282–287.

7. APPENDICES

7.1. Appendix Tables

Appendix Table 1. Experimental data for point of zero charge determination

Adjusted PH	Initial pH	Final PH	Change in pH (ΔpH)
2.01	2.07	3.13	1.06
2.99	3.81	4.70	0.89
4.01	4.73	4.97	0.24
5.00	4.70	5.00	0.30
6.01	4.87	5.02	0.15
7.00	4.87	5.00	0.13
8.00	5.08	5.09	0.01
8.99	5.53	5.28	-0.25
10.00	6.80	5.71	-1.09
11.01	7.33	5.97	-1.34
12.00	9.58	7.99	-1.59

Appendix Table 2. Co/Ct versus time for photocatalytic degradation of MB using PANI, TMP, PANI/TMP photocatalysts under visible irradiation Dye initial concentration 10 ppm, photocatalyst lode 100mgL^{-1} without pH adjustment.

Time(min)	C_t/C_o PANI	C_t/C_o TMP	C_t/C_o PANI-TMP
-30	1	1	1
0	0.97	0.99	0.95
20	0.94	0.96	0.79
40	0.91	0.94	0.73
80	0.83	0.9	0.56
100	0.73	0.85	0.52
120	0.69	0.83	0.52
140	0.66	0.77	0.5
160	0.65	0.75	0.45
180	0.65	0.74	0.39

Appendix Table 3. Co/Ct versus time for photocatalytic degradation of MB using and PANI/ TMP photocatalysts under visible irradiation (Dye initial concentration10 pp p photocatalyst lode 100 mgL^{-1} and at different pH

Time(min)	Ct/Co pH =2	Ct/Co pH= 4	Ct/Co pH= 6	Ct/Co pH = 8	Ct/Co pH = 10	Ct/Co pH = 12
-30	1	1	1	1	1	1
0	0.98	095	0.82	0.90	0.98	0.99
20	0.96	0.93	0.79	0.84	0.97	0.97
40	0.89	0.87	0.72	0.74	0.95	0.91
60	0.82	0.81	0.63	0.73	0.94	0.86
80	0.77	0.71	0.56	0.67	0.93	0.77
100	0.71	0.7	0.56	0.66	0.84	0.75
120	0.67	0.64	0.52	0.62	0.79	0.67
140	0.63	0.61	0.45	0.6	0.76	0.67
160	0.58	0.55	0.27	0.53	0.69	0.64
180	0.54	0.51	0.27	0.48	0.68	0.63

Appendix Table 4. Ct/Co of MB at different catalyst load under visible irradiation keeping pH and dye concentration as constant. Catalyst load 10, 50, 100 200 and 400 mg/L dye concentration 10 ppm at pH 8

Time(min)	Ct/Co 10mg/L	Ct/Co 50mg/L	Ct/Co 100mg/L	Ct/Co 200mg/L	Ct/Co 400mg/L
-30	1	1	1	1	1
0	0.98	0.94	0.92	0.93	0.96
20	0.94	0.85	0.83	0.84	0.9
40	0.92	0.85	0.73	0.86	0.81
60	0.86	0.76	0.63	0.75	0.77
80	0.79	0.73	0.63	0.70	0.76
100	0.74	0.72	0.56	0.66	0.73
120	0.72	0.67	0.48	0.63	0.71
140	0.7	0.64	0.42	0.56	0.66
160	0.64	0.55	0.35	0.50	0.52
180	0.54	0.50	0.27	0.40	0.47

Appendix Table 5. Ct/Co of MB dyes under visible irradiation using PANI /TMP photocatalyst at different initial dye concentration. Catalyst load= 100 gm., at pH = 8

Time(min)	Ct/Co 10 ppm	Ct/Co 15 ppm	Ct/Co 20 ppm	Ct/Co 25 ppm	Ct/Co 30 ppm
-30	1	1	1	1	1
0	0.92	0,96	0.97	0.98	0.99
20	0.85	0.93	0.94	0.95	0.96
40	0.73	0.77	0.80	0.86	0.92
60	0.64	0.70	0.74	0.8	0.88
80	0.52	0.67	0.70	0.74	0.82
100	0.45	0.52	0.63	0.70	0.74
120	0.41	0.50	0.52	0.62	0.69
140	0.40	0.45	0.51	0.55	0.66
160	0.36	0.40	0.49	0.54	0.63
180	0.27	0.37	0.42	0.56	0.61

Appendix Table 6. Ct/Co of MB in different scavengers using, PANI /TMP photocatalyst under visible irradiation as function of time. At PH = 8, Catalyst load = 100 Mg, initial dye concentration = 10ppm

Time(min)	Ct/Co $AgNO_3$	Ct/Co CH_3OH/H_2	Ct/Co $NaHCO_3$	Ct/Co Without scavenger
-30	1	1	1	1
0	0.98	0.96	0.95	0.92
20	0.89	0.83	0.85	0.85
40	0.82	0.81	0.77	0.73
60	0.76	0.72	0.67	0.64
80	0.65	0.65	0.62	0.52
100	0.57	0.55	0.51	0.45
120	0.54	0.5	0.47	0.41
140	0.52	0.46	0.45	0.40
160	0.50	0.45	0.42	0.36
180	0.47	0.4	0.35	0.27